Characterization of a group of specialized cardiomyocytes and their interaction with sympathetic neurons in murine heart

A thesis submitted to the University of Oxford for the degree of M.Sc.

Department of Pharmacology

Word Count: 11256

Kaizhong Duan

Supervised by Prof. Ming Lei

Department of Pharmacology

The University of Oxford

Table of Contents

Table of Contents....1

List of Figures....5

Declaration and Copyright....7

Abstract....8

Chapter 1. Introduction....9

1.1 PdCMs and physiological background of heart....9

1.1.1 Pnmt+ cell derived cardiomyocytes (PdCMs)....9

1.1.2 Adrenaline and noradrenaline in the heart....10

1.1.3 Potential function of PdCMs....12

1.1.4 VMAT2 and Extra-cellular Vesicles in the heart....13

1.1.5 Sympathetic innervation in the heart....14

1.2 Optogenetic technology in cardiac research....15

Chapter 2. Methods....17

2.1 $Pnmt^{Cre/ChR2}$ mice....17

2.2 Genotyping for Maintaining $Pnmt^{Cre/ChR2}$ mice line....17

2.2.1 Genomic DNA extraction....17

2.2.2 PCR for the DNA samples....18

2.2.3 PCR product check: electrophoresis on agarose gel....19

2.3 Immunohistochemical and imaging for cardiac tissue....20

2.3.1 Heart tissue preparation....20

2.3.2 Immunostaining and imaging for tissue sections....21

2.3.3 HRP-DAB staining and imaging for tissue sections..... 22
2.3.4 Immunostaining and imaging for atrial tissue..... 23
2.4 Immunohistochemical and imaging for cardiac tissue..... 24
2.4.1 Single cell isolation of ventricular myocytes..... 24
2.4.2 Immunostaining of isolated cardiomyocytes..... 25
2.4.3 Imaging of isolated cardiomyocytes..... 25
2.5 Tissue clearing for whole heart imaging..... 26
2.5.1 BABB clearing..... 26
2.5.2 CLARITY clearing..... 27
2.6 Imaging systems applied in the project..... 28
2.6.1 Optical microscopy..... 28
2.6.2 Spinning disk con-focal microscopy..... 29
2.6.3 Wide-field fluorescence microscopy..... 30
2.6.4 Light sheet fluorescence microscopy..... 31
2.7 Optical mapping..... 32
2.7.1 Optical mapping of cardiac slices..... 32
2.7.2 Data analysis and statistics..... 32
Chapter 3. Identification of a subtype of PdCMs possessing vesicular structures..... 33
3.1 Introduction..... 33
3.2 Results..... 33
3.2.1 VMAT2 staining on ventricular tissue..... 34
3.2.2 VMAT2/aACT co-staining on ventricular tissue..... 35
3.3 Discussion..... 38

Chapter 4. Identification of the innervation of sympathetic neuron and the distribution of EMT/VMAT transporters in the heart 39

4.1 Introduction 39

4.2 Results 39

4.2.1 TH immunostaining on ventricular tissue 39

4.2.2 OCT3 immunostaining on ventricular tissue sections 42

4.3 Discussion 44

Chapter 5. Light-sheet Imaging study of the distribution and function study of PdCMs in PnmtCre/ChR2 murine heart tissue by optogenetic stimulation 45

5.1 Introduction 45

5.2 Results 45

5.2.1 Light-sheet Imaging of atrial tissue dissected from $Pnmt^{Cre/ChR2}$ heart 45

5.2.2 Optimization of murine cardiac slice methodology 47

5.2.3 Vm and CaT measurements in $Pnmt^{Cre/ChR2}$ ventricle slices 48

5.3 Discussion 50

Chapter 6. General Discussion 51

6.1 Optimization of the genotyping protocol 51

6.2 Distribution of PdCMs by light-sheet imaging 51

6.3 OCT3 and TH staining on ventricular tissue sections 52

6.4 VMAT2/aACT staining on cardiac tissue sections and cellular vesicles 53

6.5 Optic mapping on heart tissue.....54

6.6 Conclusion and future prospective.....55

References.....56

List of Figures and Charts

Chapter 1

Figure 1.1: Schematic diagram demonstrating cell-type specific expression of ChR2-tdTomato under a *Pnmt* promoter.
Figure 1.2: Distribution pattern of PdCMs.
Figure 1.3: Noradrenaline Synaptic Pathway and two uptake mechanisms.
Figure 1.4: Hypothesis of PdCMs mediated Regulation between Sympathetic Neuron Cells and conventional Cardiomyocytes.
Figure 1.5: Sympathetic neuron innervation pattern in the heart.
Figure 1.6: A simplified schematic diagram of equipment for optogenetic studies.

Chapter 2

Table 2.1: Recipe for PCR mixture
Figure 2.1: Genotyping of Optogenetic mice.
Table 2.2: Recipe for Kreb's solution
Table 2.3: Recipe for Cell isolation solution
Figure 2.2: A cut-away diagram for Zeiss optical microscope
Figure 2.3: Light pathways in con-focal microscopy
Figure 2.4: Yokogawa Spinning Disk unit optical configuration
Figure 2.5: Schematic diagram of wide-field fluorescence microscopy
Figure 2.6: Schematic diagram of light sheet fluorescence microscopy and light pathways

Chapter 3

Figure 3.1: VMAT2 staining on ventricular tissue sections
Figure 3.2: Reconstructed 3D model for VMAT2/aACT co-staining on ventricular tissue
Figure 3.3: Intra-cellular vesicle structure by VMAT2/aACT co-staining

Chapter 4

Figure 4.1: TH immunostaining on adrenal gland, brain and ventricular tissue
Figure 4.2: Innervation in heart tissue revealed by VMAT2 staining
Figure 4.3: OCT3 immunostaining on Olfactry bulb and ventricular tissue sections (3D reconstructed model)

Chapter 5

Figure 5.1: Light-sheet Imaging of atrial tissue dissected from $Pnmt^{Cre/ChR2}$ heart
Figure 5.2: Optimization of murine cardiac slice methodology
Figure 5.3: Vm and CaT measurements in murine ventricle slices

Figure 5.4: Transmural and regional distribution of AP duration under different light intensity stimulation
Figure 5.5: Activation patterns for before and during optogenetic pacing
Figure 5.6: Amplitude Maps for Sinus node 200Hz pacing

Declaration and Copyright

I confirm that all the research and findings presented in the thesis are my own work unless otherwise indicated clearly.

The author of this thesis (including any appendices and/or schedules to this thesis) owns any copyright in it. He has given the University of Oxford the rights to use Copyright for any administrative, promotional, educational and/or teaching purposes. The ownership of any patents, designs, trademarks and any other intellectual property rights except for the copyright and any reproductions of copyright works, for example graphs and tables, which may be described in this thesis, may not be owned by the author and may be owned by third parties. Such intellectual property rights and reproductions cannot and must not be made available for use without prior written permission of the owner of the relevant intellectual property rights.

Abstract

Our group recently described a distinctive, novel class of $Pnmt^{+}$ cell-derived cardiomyocytes (PdCMs), with a potential endocrine role. However, our understanding of this new cardiomyocyte population is still very limited. There are numerous issues to be addressed such as the evidence of their endocrine machinery, their interaction with autonomic system, and their physiological function in the heart corresponding to their unique location in the heart. In order to address these issues, by using wild type and $Pnmt^{cre/ChR2}$ mice as model systems, I have conducted a series of immunohistochemical and electrophysiological experiments with the aims of: i) exploring the potential endocrine machinery of PdCMs (Chapter 3); ii) clarifying their interaction with sympathetic neuron innervation (Chapter 4), and iii) determining their physiological role in the atria (Chapter 5).

The key findings of this report include: i) firstly, a subtype of PdCMs containing vesicular structures was revealed by using immunostaining of vesicular monoamine transporter 2 (VMAT2) and myocyte marker α-actinin (aACT) as well as extra-neuronal monoamine transporter (EMT/ OCT3). This is the first time that such cellular vesicles have been found in cardiomyocytes. Although such vesicular structure requires further investigation, it opens a new frontier for exploring the cardiomyocyte endocrine function; ii) secondly, a synapse-like junction structure between these cardiomyocytes and sympathetic neuron innervation was identified by the staining of anti-Tyrosine Hydroxylase(TH) and anti-VMAT2; iii) finally, by using optogenetic stimulation combining with a high resolution optical imaging, the potential role as alternative pacemaker site of PdCMs was explored, which was induced by optogenetic pacing technique.

In conclusion, the results presented in my report have provided novel evidence to suggest the endocrine function and the pivotal role in neurocardiac crosstalk of PdCMs.

Chapter 1. Introduction

1.1 PdCMs and physiological background of heart

1.1.1 Pnmt⁺ cell derived cardiomyocytes(PdCMs) expressing channelrhodopsin ChR2

Phenylethanolamine N-methyltransferase (Pnmt) is an enzyme found primarily in endocrine cells presented in the adrenal medulla that converts norepinephrine (noradrenaline) to epinephrine (adrenaline)[1]. It is also expressed in small groups of neurons in specific regions of the brain. Channelrhodopsins are a subfamily of retinylidene proteins (rhodopsins) that function as light-gated ion channels. They enable light to control electrical excitability, intracellular acidity, calcium influx, and other cellular processes[2]. Channelrhodopsin-1 (ChR1) and Channelrhodopsin-2 (ChR2) from the model organism Chlamydomonas reinhardtii are the first discovered channel rhodopsins.

In previous studies conducted in our laboratory, channel rhodopsin 2 (ChR2) was specifically introduced into murine cells expressing the Pnmt gene. When tracing Pnmt expressing cells in the heart, significant numbers of cardiomyocytes were found to be derived from Pnmt derived cells. These special types of myocytes were then defined as PdCMs (PNMT derived cardiomyocytes) in a recently published paper from our group[3].

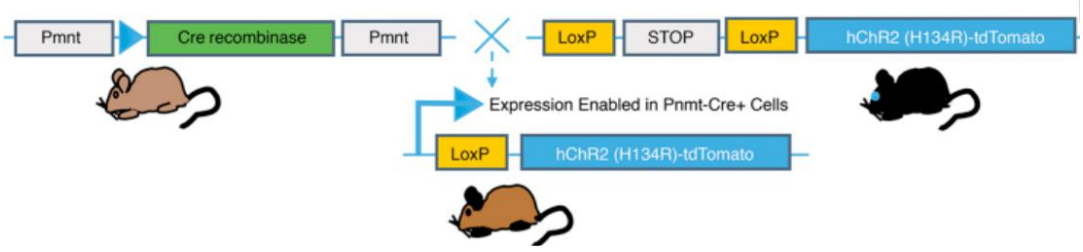


Figure 1.1 Schematic diagram demonstrating cell-type specific expression of ChR2-tdTomato under a *Pnmt* promoter. (Wang *et al.*, 2017)[3]

Figure 1.1[3] gives the schematic diagram demonstrating how the *Pnmt*$^{Cre/ChR2}$ was generated in our lab by crossing a Cre-Pnmt mouse line with a Loxp-ChR2-tdTomato mouse line.

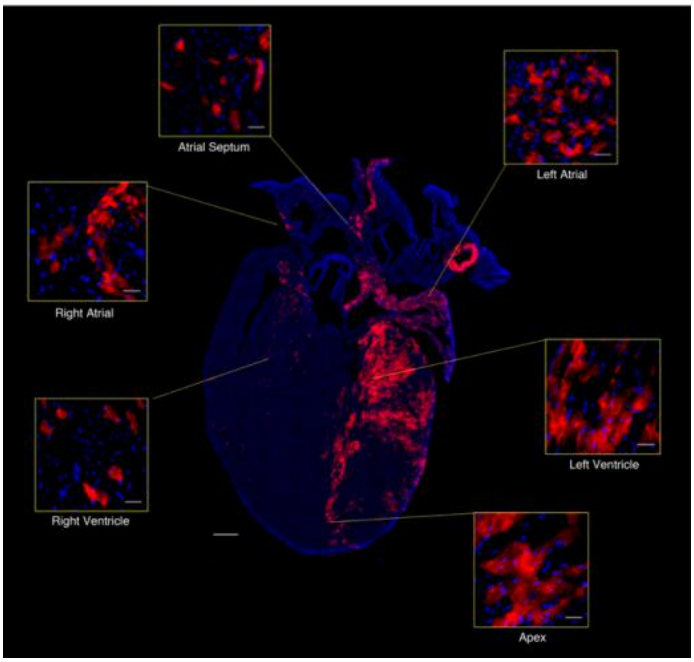


Figure 1.2 Distribution pattern of PdCMs. (Wang *et al.*, 2017)[3] A representative image showing tdTomato fluorescence of the coronal section taken from an adult *Pnmt*$^{Cre/ChR2}$ mouse heart, with inserts showing the tdTomato fluorescence in different regions of the heart. Scale bar: 100 μm.

As has been shown on **figure 1.2**[3], PdCMs are found to be predominantly expressed in the left side of the heart (left atrium and left ventricle) and the conduction system such as the sinus node and AV node, indicating the potential important role of PdCMs in particular regions. Blue light (~470nm wavelength) pulses were used to selectively stimulate these cells by activating ChR2 channels in adult Pnmt-Cre/ChR2 hearts and spatiotemporally controlled stimulation of PdCMs in intact heart was achieved. The PdCMs are similar to conventional cardiomyocytes in morphological, electrical and contractile properties. However, the specific function of this group of cells remains largely unknown.

Over the past few years, several groups have reported the important roles specific cardiac sub-population and sympathetic nervous system in cardiac regeneration and sympathetic re-innervation[4,5,6]. Therefore, it is worth researching on the function of PdCMs.

1.1.2 *Adrenaline and noradrenaline in the heart*

Adrenaline[7], also known as adrenalin or epinephrine is usually produced by both the adrenal glands and certain neurons[8]. Adrenaline binds to both alpha and beta receptors of the target tissues[9].

Noradrenaline, also known as Norepinephrine (NE) or noradrenalin, plays important roles in mobilizing the brain and body for action. Noradrenaline release is lowest during sleep, rises during wakefulness, and reaches much higher levels during situations of stress or danger. Both adrenaline and noradrenaline are hormones and neurotransmitters in the catecholamine family. They both play very important roles in fight-or-flight response. In the response, they can increase blood flow to muscles, output of the heart, pupil dilation response, and blood sugar level[9,10].

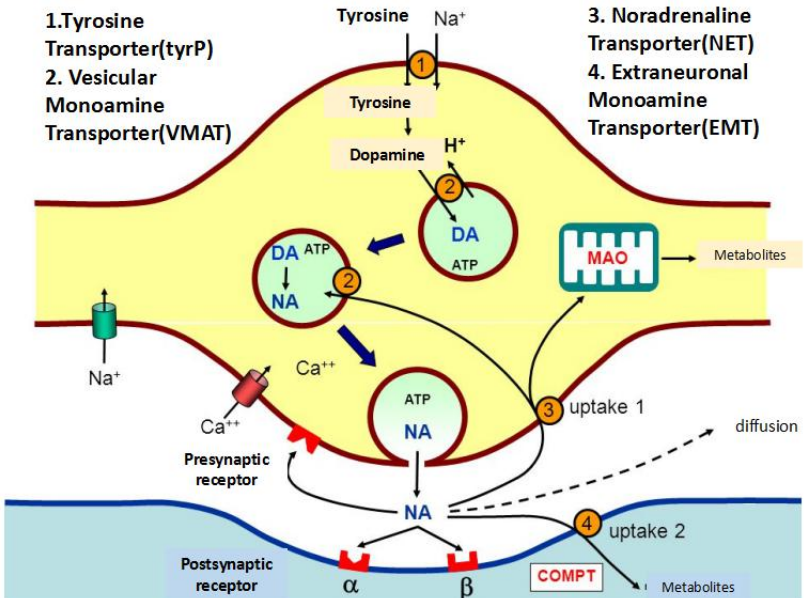


Figure 1.3 Noradrenaline Synaptic Pathway and two uptake mechanisms. (Waller and Sampson, 2017)[11]

Figure 1.3[11] briefly indicates the noradrenaline synaptic pathways and two uptake mechanisms. As is shown, noradrenaline can be converted from adrenaline by PNMT and degraded by Catechol-O-transferase (COMT) and monoamine oxidase (MAO).

The heart can receive signals from both parasympathetic nerves and sympathetic nerves. The former are responsible for decreasing heart rate and the latter are responsible for increasing the heart rate, conduction and force of contraction.

Adrenaline and noradrenaline enhance contractile force through both atrial and ventricular beta 1-adrenoceptors. Adrenaline can also enhance contractile force through atrial beta 2-adrenoceptors. In the ventricle, adrenaline increases force via beta 2-adrenoceptors by up to 60% of its maximal beta 1 response. Noradrenaline can increase atrial and ventricular contractile force through beta 2-adrenoceptors but only at high concentrations[12].

1.1.3 Potential function of PdCMs

Organic cation transporter 3 (OCT3) or Extra-neuronal monoamine transporter (EMT) is a protein that in humans is encoded by the SLC22A3 gene[13,14,15]. OCT3 is widely distributed in brain tissue. It is also reported to be expressed in the heart[16].

In the noradrenaline synaptic pathway, as has been demonstrated in **Chapter 1.1.2** and **Figure 1.3**, noradrenaline binds to and activates α and β receptors. After an action potential, the noradrenaline molecules quickly become unbound from their receptors. They are then absorbed back into the presynaptic cell, mediated primarily by the noradrenaline transporter. Once back into the cytosol, noradrenaline can either be broken down by monoamine oxidase[17](MAO) or repackaged into vesicles by vesicular monoamine transporter (VMAT), making it available for future release. This neuronal transmitter re-uptake mechanism is called uptake-1. In addition about 25% of the noradrenaline molecules are absorbed by the extra-neuronal monoamine transporter(EMT) in peripheral cells

to prevent lateral diffusion of transmitter, in a mechanism known as uptake-2[18]. Such extra-neuronal uptake mechanisms occur in both muscle cells[19], and in the heart[20].

Based on the previous study of PdCMs, there could be possibilities that PdCMs play an important role as a mediator between conventional myocytes and sympathetic neurons. They may convert noradrenaline absorbed via uptake-2 mechanism to adrenaline. The hypothesis has been converted into diagram shown as **Figure 1.4**.

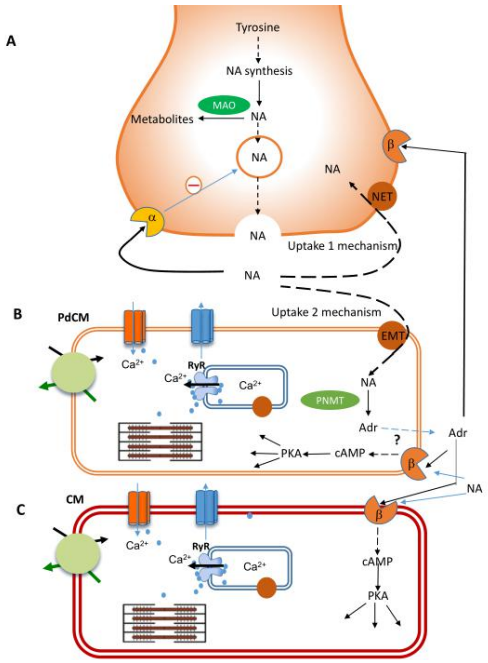


Figure 1.4 Hypothesis of PdCMs mediated Regulation between Sympathetic Neuron Cells and conventional Cardiomyocytes.

1.1.4 VMAT2 and Extra-cellular Vesicles in the heart

The vesicular monoamine transporter (VMAT) is a transport protein integrated into the membrane of synaptic vesicles of presynaptic neurons[21]. It transports monoamine neurotransmitters – such as dopamine, serotonin, norepinephrine, epinephrine, and histamine – into the vesicles, which release the neurotransmitters into synapses as chemical messages to post-synaptic neurons. There are two types of VMATs widely expressed in mammals: VMAT1 and VMAT2[22]. VMAT1 is expressed mainly in large dense-core vesicles (LDCVs) of the peripheral nervous system. VMAT2 favors expression in a variety of monoaminergic cells of the CNS such as the brain, sympathetic nervous system and mast cells. Over the years, VMAT2 has been widely used as

the marker for vesicles and the pharmacological target[23,24]. VMAT2 was also used for studying the cardiac neural structure[25].

Recently, cardiac vesicles have attracted scientific attention. Extra-cellular vesicles demonstrated in the heart may be important in some cardiovascular pathology[26,27]. They may function in cardioprotection[28,29]. Their contained microRNAs have been subjects of interest[30].

Containing monoamine neurotransmitters, these vesicles are indispensable in sympathetic signaling and cardiac disease mediating with no doubt[31,32]. Intra-cellular vesicles, however, have not been well studied and no intra-cellular vesicles have been reported in the heart.

1.1.5 Sympathetic innervation in the heart

The dysfunction of autonomic control of the heart play an important role in the development of life-threatening arrhythmias that can lead to sudden cardiac death. Sympathetic activity is up-regulated during these conditions and the sympathetic nerves present a target for treatment[33]. In mammals including humans, the cardiac preganglionic cell bodies are located in the grey matter of the first six segments of the thoracic spinal cord. The majority of the cardiac sympathetic innervation arises from these ganglia although a few post-ganglionic cell bodies have been described in the myocardium. These neurons modulate chronotropy, dromotropy, lusitropy and inotropy functions in all the cardiac chambers. The innervating sympathetic neurons are proved to be the regulator of heart size and cardiomyocyte cell cycle[34]. Shown on **Figure 1.5**[35]

is a schematic diagram of sympathetic neuron innervation in the heart, which was acquired by scientists(K. Shivkumar, *et al*, 2016) from UCLA and Caltech.

In my project, staining procedures for tyrosine hydroxylase(TH) and VMAT2 were applied to identify the innervation pattern of the heart tissue and images were taken by confocal microscope.

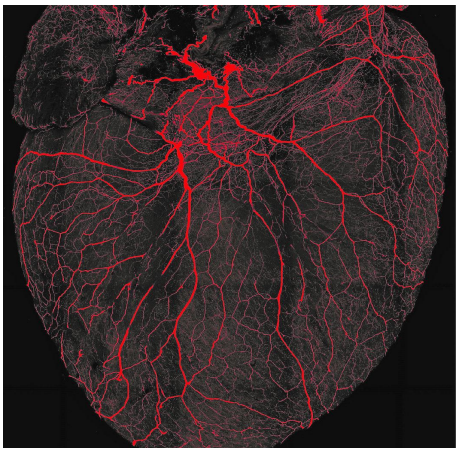


Figure 1.5 Sympathetic neuron innervation pattern in the heart. (K. Shivkumar, et al,, 2016)[35]

1.2. Optogenetic technology in cardiac research

Optogenetics provides a biological technique that involves the use of light to control cells in living tissue, typically neurons that have been genetically modified to express light-sensitive ion channels. It is a neuromodulation method that uses a combination of techniques from optics and genetics to control and monitor the activities of individual neurons in living tissue and to precisely measure these manipulation effects in real-time[36]. The optogenetic techniques were first utilized in mammalian neurons in 2005[37], and soon became a useful tool in cardiac research[38,39,40]. In our study, I performed measurements of intracellular Ca^{2+},CaT, and cell membrane potential, Vm with high resolution mapping, followed by AP duration analysis. The mapping methods were optimized by Q Wen and K Gandhi in our lab in previous studies.

Given that PdCMs may play important roles in cardiac adrenergic signaling, I proposed a hypothesis that PdCMs can uptake noradrenaline through uptake2 mechanism. They convert Noradrenaline to Adrenaline by PNMT enzyme.

Adrenaline molecules are then released and could target both neuron cells and cardiomyocytes to activate protein kinase A. Therefore, EMT transporters would be possibly located on the membrane of PdCMs.

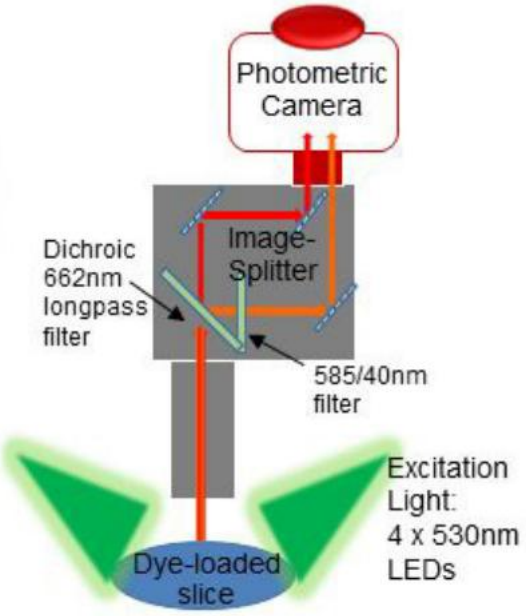


Figure 1.6 A simplified schematic diagram of equipment for optogenetic studies.

Given in **Figure 1.6** is a schematic diagram of equipment for optogenetic studies, which indicates the simplified system for stimulating samples and observing signals in optogenetic studies.

Chapter 2. Methods

2.1 Pnmt$^{Cre/ChR2}$ mice

The existing mouse line was previously generated by crossing Pnmt-Cre mice with B6. Cg-Gt (ROSA) 26Sortm27.1(CAG-COP4H134R/tdTomato) Hze/J strain (Stock No. 012567, Jackson Labs) (Wang *et al.*, 2017)[3]. In this mouse model, PdCMs are linked with Channelrhodopsin-2 (ChR2) and labeled with tdTomato fluorophore. Pnmt-Cre positive/ tdTomato-ChR2 positive mice were selected as breeding pairs to breed mouse colonies.

2.2 Genotyping for Maintaining Pnmt$^{cre/ChR2}$ mice line

The ear/tail clips of mice aging from 2 weeks to 6 weeks were collected by Richard Corderoy in animal centre of Department of Pharmacology. There were over 100 mice in 6 generations were performed with genotyping in order to identify the genotype of mouse colonies. Cre primers and tdTomato primers were used during PCR procedure separately.

2.2.1 Genomic DNA extraction

Ear clips or tail samples were collected with the help of Biomedical Service of University of Oxford. Proteinase K mixture were prepared by mixing 500 ml lysis buffer per sample plus 5 ml proteinase K per ear sample (6 ml proteinase K per tail sample). The samples in eppendorff tube were added with proteinase K

mixture and heated at 55°C overnight on heating block. The next day, 500 ml of chloroform (Use phenol: chloroform 25:24 and take only the bottom layer which is chloroform.) was added to each sample after vortex. The samples were then centrifuged at 13,000 rpm for 5 minutes, followed by pipetting off the upper aqueous layer and transferring into appropriated tubes. 500 ml ice cold isopropanol was added into each sample, followed by fully vortex. The samples were centrifuged at 4°C 13,000 rpm for 30 minutes to precipitate the DNA. A pellet was formed at the bottom of each tube. The supernatant solution was removed with the help of pipette. The pellet was suspended in 70% ethanol to wash before centrifuging at 4°C 13,000 rpm for 5 minutes. Afterwards, the ethanol was tipped off, with the pellet leaving inside. The pellet was dried with lid open at room temperature then in heating block at 37°C for 10 minutes. The pellet collected from ear samples was suspended in 100 ml injection water (120 ml of injection water for tail samples) and dissolved at 55°C for 60 minutes.

2.2.2 PCR for the DNA samples

The primer mix (10 ml forward primer + 10 ml reverse primer + 80ml injection water) was freshly made-up and the PCR mixture was prepared with the recipe shown in **Table 2.1**.

Table 2.1 Recipe for PCR mixture

Reagents for PCR mixture	**Volume (ml per sample)**
PCR master mix	5
RNAse free water	2
Coral red	1
Primer mix	1
Total volume	9

PCR tubes were labeled for each sample with 9 ml PCR mixture added. 1 ml of DNA sample was then loaded into each tube to give a total volume of 10 ml. The PCR tubes was then transferred into PCR machine with lips covered. The PCR machine was started to select respective program. The program 061113 was for Cre and 081113 was for ChR2.

2.2.3 PCR product check: electrophoresis on agarose gel

1.2% agarose gel mixture was prepared with 1.92g agarose and 160 ml 1 x TAE buffer. Microwave oven was used to heat the mixture for dissolving. 3.2 ml of ethidium bromide was added into the mixture after cooling down to approximately 55°C.

The mixture was then poured into the gel mould with combs in. Bubbled were removed by using pipette tips. Combs were removed after 30 minutes of cooling and setting, followed by filling the electrophoresis tank with used TAE buffer.

The gel was run at 100V for approximately 30 minutes before taking photos under UV imager.

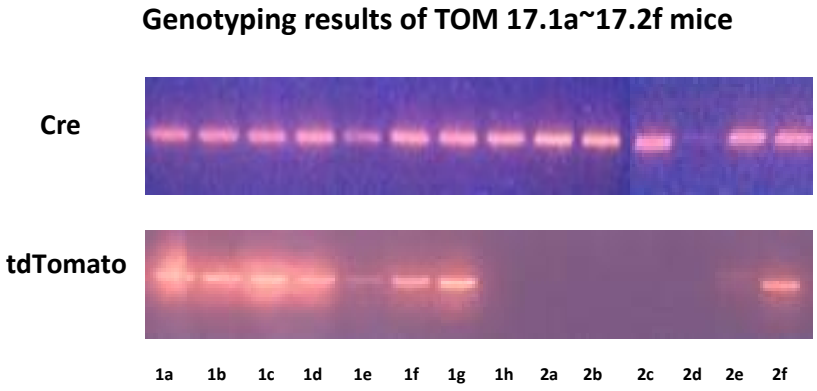


Figure 2.1 Genotyping of Optogenetic mice. PCR was performed to identify the genotype of the mice. Ethidium bromide was loaded into the agarose gel as dye and the images were obtained under 302nm ~ 365nm laser visualizer.

Take the TOM.17 generation as an illustration, totally 14 mice were tested by Cre and tdTomato. As is shown on **Figure 2.1**, Cre gene was expressed in all mice except for TOM 17.2d. As for tdTomato, the expression level in TOM 17.1a, 1b, 1c, 1d, 1f, 1g and 2f were comparatively high against TOM 17.1e and 2e, other mice did not express tdTomato gene. Therefore, the Pnmt-Cre positive/ tdTomato-ChR2 positive mice were identified to be TOM 17.1a, 1b, 1c, 1d, 1f, 1g and 2f, and these mice were defined as optogenetic mice and selected for following experiments. Other mice, however, were used for optimizing the methodology.

2.3 Immunohistochemical and imaging for cardiac tissue

2.3.1 Heart tissue preparation

Table 2.2 Recipe for Kreb's solution

Reagents for Kreb's solution	**g/L**	**g/2L**	**g/5L**
NaCl	6.95	13.9	34.75
NaHCO3	2.10	4.20	10.50
Glucose	1.8	3.6	9.0
Na Pyruvate	0.2	0.4	1.0
KCl	0.2982	0.5964	1.4910
1M MgCl2(ml)	1.0	2.0	5.0
KH2PO4	0.1633	0.3266	0.8165
1M CaCl2(ml)	1.8	3.6	9.0

The selected mice were injected with overdose of 1.2% avertin solution (0.5~0.8 ml IP (2, 2, 2-Tribromoethanol, Sigma-Aldrich) and heparin (200 units) 5 minutes before dissection in accordance with schedule 1 killing method. The hearts were then collected.

Each freshly isolated heart was placed in PBS and the aortic stem was kept intact for cannulation. The heart was then moved under dissecting microscope and 22G cannula was inserted into aortic stem and tied on Langendorff system.

Kreb's solution was used to gently perfuse the heart in order to flush out blood (the tip of cannula should above aortic valve for retrograde perfusion), followed by PBS perfusion. 3-5 ml of 4% para-formaldehyde in PBS solution was gently perfused with a switched syringe to fix the tissue.

The tissue was then incubated at 4°C in 4% para-formaldehyde in PBS overnight for post-fix. Then, the tissue was transferred to 30% sucrose in PBS containing 0.02% sodium azide and store at 4 °C until ready for sectioning. The Kreb's solution was made with the recipe shown in **Table 2.2**.

The prepared heart was placed on sectioning machine and fixed with adhesive gel. Sections were acquired by handling the machine and the thickness for each section was between 20 nm and 50 nm according to the tissue structure of the particular regions.

2.3.2 Immunostaining and imaging for tissue sections

The sliced tissue sections were washed in PB solution 10 minutes twice, followed by 10 minutes wash in TBS+Tx solution. After wash, the sections were blocked for 1 hour at room temperature in TBS+Tx+20%NHS (normal horse serum).

Primary antibody diluted in TBS+Tx+1%NHS was applied and incubated on shaker

for 3 days at 4 °C. The sections were then transferred into secondary antibody in TBS+Tx+1%NHS before 3 times wash with TBS+Tx for 10 minutes. After overnight secondary antibody incubation, the slices were washed 3 times with TBS+Tx for 10 minutes each time.

The tissue was then mounted on slides with mounting medium and the cover slips were sealed with nail vanish. Both positive controls and negative controls were prepared at the same time. The slides were imaged under spinning disk con-focal microscope and wide-field fluorescence microscope. (The imaging systems used in the experiments are introduced in **Chapter 2.6.2** and **Charpter 2.6.3**)

2.3.3 HRP-DAB staining and imaging for tissue sections

The tissue sections sliced were first rinsed twice in PBST (PBS-Tween 20) for 2min, before 30min serum blocking. The species of the serum for incubating was same as secondary antibody. Avidin/biotin block was done after normal serum block. Primary antibody in TBST+1%NHS was then applied for overnight at 4 °C, followed by PBST wash for 3 times, 10min each wash.

After incubation in peroxidase blocking solution for 10 minutes at room temperature, the tissue was incubated with biotinylated secondary antibody in TBST+1%NHS for 30 minutes at room temperature. 3 times of 10min PBST wash was followed before the sections were transferred into streptavidin-HRP in PBS for 30 minutes at room temperature. Another 3 times of 10min PBST wash was required before incubating in DAB solution for 3 minutes. After incubation, 3 times of 10 min PBST wash was performed, followed by distilled water rinse.

The tissue was dehydrated through 95% ethanol for 2min and 100% ethanol for

2x3min. Then the tissue was mounted with mounting medium after clearing in xylene for 2x5min. The cover slips were sealed with nail vanish and the slides were stored at room temperature. Optical microscope was used to image the slides. (The optical microscope imaging system applied in this experiment is introduced in **Chapter 2.6.1**)

2.3.4 Immunostaining and imaging for atrial tissue

Freshly isolated heart from mouse with the age of 8-20 weeks was placed in PBS and the aortic stem was kept intact for cannulation. The heart was then moved under dissecting microscope and 22G cannula was inserted into aortic stem and tied on Langendorff system.

After perfusion with Kreb's solution and PBS solution, the heart was dissected to acquire target atrial tissue. The tissue was fixed in 4% para-formaldehyde in PBS solution at 4°C for 4 hours. The atrial tissue was washed in PBS solution 10 minutes for 3 times, followed by 1 hour blocking in PBS+10%NHS at room temperature. Primary antibody diluted in PBS+1%NHS was applied and incubated on shaker overnight at 4°C.

The tissue was then transferred into secondary antibody in PBS+1%NHS before 3 times wash with PBS for 10 minutes each. After 4 hours secondary antibody incubation, the tissue was washed 3 times with PBS for 10 minutes each time.

The tissue was then stored in PBS before imaging. Light-sheet microscope was applied to image the whole piece of tissue. (The light-sheet imaging system is introduced in **Chapter 2.6.4**)

2.4 Immunostaining and imaging for single cells

2.4.1 Single cell isolation of ventricular myocytes

Mice used in the experiments were sacrificed via cervical dislocation in accordance with schedule 1 killing method.

Hearts were rapidly excised and Langendorff-perfused with oxygenated Krebs solution at 37°C and at constant rate of 3.5-4 ml/min for 10 min. To prevent formation of blood clots in the coronary circulatory system, animals were treated with heparin under non-recovery terminal general anesthesia by injection of overdose of 1.2% avertin solution prior to sacrifice after organ excision according to approved procedure by the Home Office.

Cell Isolation solution was used to perfuse the heart to flush off the blood, followed by enzyme solution (20mg collagenase II diluted in 40ml isolation solution) perfusion at 37°C for 5.5-7.5 minutes until the heart was fully digested. The recipe for cell isolation solution is shown in **Table 3.3**.

Table 3.3 Recipe for Cell isolation solution

Reagents for Cell Isolation Solution	**g/L**
NaCl	7.8
HEPES	2.38
Glucose	2.0
Na_2HPO_4	0.065
$MgSO_4$(1M)	1.2 ml
KCl	0.402

The heart was moved into taurine solution to terminate the enzyme digesting and then diced into small pieces. The isolated cells were acquired by blowing-suction using the dropper. The mixture containing myocytes were filtered through a filter paper and collected in 15 ml centrifuge tubes. The cells were washed with BSA buffer (0.2g BSA diluted in 200ml isolation solution) for 3x3min at 350g/min centrifuge.

2.4.2 Immunostaining of isolated cardiomyocytes

The isolated cells were placed on slides and fixed in 4% PFA for 30 min. After washing wish PBS (0.01M phosphate buffer solution) three times at 10 min intervals, the cells were then permeabilized by incubating in PBS containing 0.1% Triton X-100 for 30 min, after which they were washed with PBS three times. 10%NHS in PBS was used for blocking for 1 hour at room temperature. The cells were then incubated with the primary antibody in 1%BSA in PBS overnight at 4°C. After washing with PBS for three time at 10 min intervals, the cells were incubated with secondary antibody diluted in 1%BSA in PBS for 1 hour at room temperature. Another three PBS washes were performed before mounting the cells with mounting medium. The cover slips were sealed with nail vanish and the slides were stored in the dark at 4°C.

2.4.3 Imaging of isolated cardiomyocytes

The slides were observed with optic microscope, spinning disk confocal microscope and wide-field microscope. Relevant training was taken before imaging in Imaging Centre in Department of Biochemistry. All the imaging

experiments were strictly followed the procedure trained in Imaging Centre and the first 3 times were under supervision of staff in Imaging Centre.

2.5 Tissue clearing for whole heart imaging

2.5.1 BABB clearing

Mice were sacrificed via cervical dislocation in accordance with schedule 1 killing method. Hearts were rapidly excised and Langendorff-perfused with oxygenated Krebs solution. at 37°C and at constant rate of 3.5-4 ml/min for 10 min.

To prevent formation of blood clots in the coronary circulatory system, animals were treated with heparin under non-recovery terminal general anesthesia by injection of overdose of 1.2% avertin solution prior to sacrifice after organ excision according to approved procedure by the Home Office.

BABB clearing solution was made by mixing benzyl alcohol (Sigma B-1042)/ benzyl benzoate (Sigma B-6630) at the ratio of 1:2. The isolated heart was dehydrated with grade MeOH series as follows:

a. 25% MeOH (25 % MeOH / 75 % PBT (PBS with 0.1% tween-20) for 5 min
b. 50% MeOH, 5 min,
c. 75% MeOH, 5 min,
d. 100% MeOH, 2x 5 min each
e. 50% MeOH - 50% BABB, 2x 5 min each
f. 25% MeOH - 75% BABB, 5 min

The heart was then immersed in BABB clearing solution at room temperature for

2-3 days until the heart became transparent. After mounting in the mounting medium with the refractive index of 1.51, the heart was observed under light-sheet microscope.

2.5.2 CLARITY clearing

The CLARITY clearing protocol (Tomer R et.al, Nature, 2014) used in the experiments is as follows:

Prepare 400 ml of HM solution by mixing 40 ml of 40% (wt./vol) acrylamide (4% (wt./vol) final concentration), 10 ml of 2% (wt./vol) bis-acrylamide (0.05% (wt./vol) final concentration), 40 ml of 10× PBS, 100 ml of 16% (wt./vol) PFA (4% (wt./vol) final concentration), 210 ml of distilled water and 1 g of VA-044 thermal initiator (0.25% (wt./vol) final concentration). Keep all the reagents on ice; divide 40 ml of the HM solution into aliquots in 50-ml conical tubes and store them at −20 °C until needed (several weeks). Acrylamide and bis-acrylamide concentration in HM solution can be proportionally reduced to speed up the clearing process.

Prepare SBC buffer stocks of 20% (wt./vol) SDS (in H2O) and 1 M boric acid buffer (pH adjusted to 8.5). Final clearing buffer is freshly prepared by diluting 20% (wt./vol) SDS and 1 M boric acid buffer fivefold in distilled water.

Transfer the air-tight closed conical tube to a 37 °C room or to a water bath for 3–4 h. Gentle shaking helps in heat transfer for achieving robust and uniform polymerization. Carefully extract the heart from solidified hydrogel by softly rubbing all the hydrogel from the surface. Kim wipes can be used to remove the residual gel from the tissue surface. Wash the tissue sample twice with 50 ml of SBC buffer for 24 h at room temperature to dialyze the remaining PFA, initiator

and monomer. Transfer the heart into a hand-made ETC chamber and run at 37°C at 25V for 5 days. Immediately change the buffer if the pH drops below 7.5. Wash the tissue twice in PBST or boric acid buffer (0.2 M/pH 8.5 with 0.1% (vol/vol) Triton X-100) for 1 d at 37 °C. Transfer the heart from boric acid/0.1% (vol/vol) Triton X-100 to PBST 30 min before incubation with primary antibody. Incubate in primary antibody/PBST solution (beginning with 1:50 dilution) at 37 °C for a week. Wash off the primary antibodies with PBST buffer at 37 °C for 3 days. Incubate with the desired secondary antibody (1:50–1:100) in PBST for 2 d at 37 °C for 1 week. Wash off the secondary antibodies with PBST at 37 °C for 3 days. Transfer the PBST-washed tissue into 87% (vol/vol) glycerol, and periodically check the visual clarity of the sample over the next few hours. Once the tissue has been fully clarified, immediately image the heart with light-sheet microscope.

2.6 Imaging systems applied in the project

2.6.1 Optical microscopy

The optical microscope, often known as the light microscope, is a type of microscope that uses visible light and a system of lenses to magnify images of small subjects[41]. Optical microscopes are the oldest design of microscope and were possibly invented in their

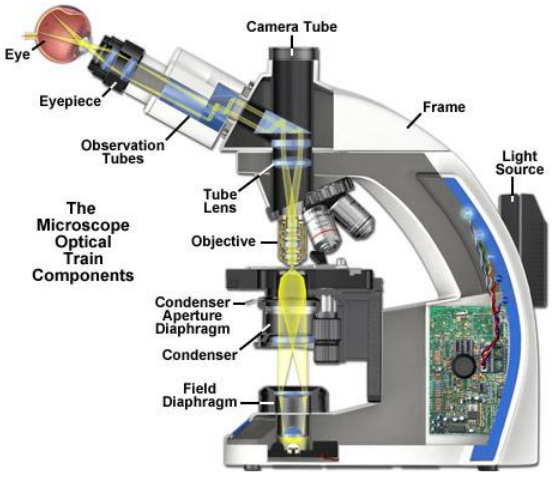


Figure 2.2 A cut-away diagram for Zeiss optical microscope. (From Zeiss Edu)[42]

present compound form in the 17th century. Over the years, with the development of technology, the optical microscopes have been much improved and optimized.

Shown in **Figure 2.2**[42] is the diagram for Zeiss optical microscope which was applied in the experiments in my project. The HRP-DAB stained cardiac tissue sections were observed under this microscope and the images taken were transferred into the computer connected with the microscope.

2.6.2 Spinning disk confocal microscopy

Confocal microscopy, also called confocal laser scanning microscopy (CLSM) or laser confocal scanning microscopy (LCSM), is an optical imaging technique for increasing optical resolution and contrast of a micrograph. The main concept of confocal microscopy in image formation is to utilize a spatial pinhole to block out-of-focus light[43]. The most important advantage of confocal microscopy against conventional fluorescent microscopy is the possibility to re-construct three-dimensional structures (a process known as optical sectioning) within an object[44]. **Figure 2.3**[45] gives the light pathways in confocal microscopy.

Spinning-disk (Nipkow disk)[47] confocal microscopes use a series of moving pinholes on a disc to scan spots of light. Since a series of pinholes scans an area in parallel, each pinhole is allowed to hover over a specific area for a longer amount of time thereby reducing the excitation

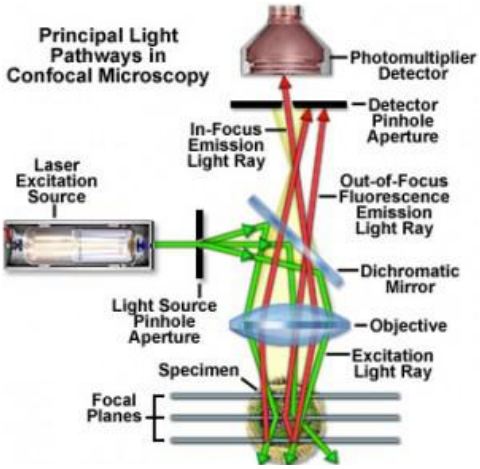


Figure 2.3 Light pathways in confocal microscopy. (From Zeiss Edu)[45]

energy needed to illuminate a sample when compared to laser scanning microscopes.

Decreased excitation energy reduces phototoxicity and photoblea c-hing of a sample often making it the preferred system for imaging live cells or organisms.

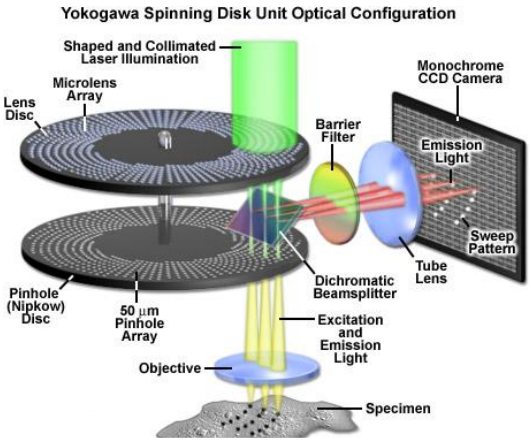


Figure 2.4 Yokogawa Spinning Disk unit optical configuration. (From Zeiss Edu)[46]

Shown in **figure 2.4**[46] is a unit optical configuration diagram of spinning disk microscope produced by Yokogawa Electric Corporation, explaining the optic units and light pathways in a spinning disk microscope.

2.6.3 Wide-field fluorescence microscopy

In wide-field microscopy, the whole specimen on the microscope stage will be exposed to a light source. As is shown in **Figure 2.5**[48], wide-field fluorescence microscopy is a very widely used technique to obtain both topographical and dynamic information. It relies on the simultaneous illumination of the whole sample. The source of light is usually a mercury lamp, giving out pure white light. Optical filters are then used in order to select the wavelength of excitation light (the excitation filter). Excitation light is directed to the sample via a dichroic mirror (ie a mirror that reflects some wavelengths but is transparent to others) and fluorescent light detected by a camera (usually a CCD camera). Thus, both the illumination and detection of light covering the whole visual field of

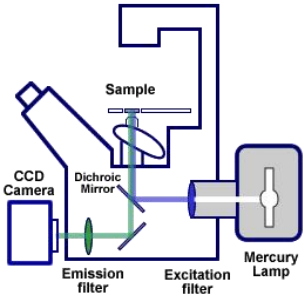


Figure 2.5 Schematic diagram of wide-field fluorescence microscopy. (From Research techniques in University of Bristol)[48]

the chosen microscope objective is achieved simultaneously.

2.6.4 Light sheet fluorescence microscopy

Light sheet fluorescence microscopy (LSFM) is a fluorescence microscopytechnique with an intermediate-to-high optical resolution, but good optical sectioning capabilities and high speed[49]. In contrast to epifluorescence microscopyonly a thin slice of the sample is illuminated perpendicularly to the direction of observation. For illumination, a laser light-sheet is used, i.e. a laser beam which is focused only in one direction. A second method uses a circular beam scanned in one direction to create the light sheet. As only the actually observed section is illuminated, this method reduces the photodamage and stress induced on a living sample. Also the good optical sectioning capability reduces the background signal and thus creates images with higher contrast, comparable to confocal microscopy. **Figure 2.6**[50] schematically explains the mechanism of light sheet fluorescence microscopy. Since LSFM scans the specimen layer by layer, the most important advantage of light-sheet fluorescence microscopy against point-scanning methods is that it makes it possible to observe large tissue blocks in rapid speed.

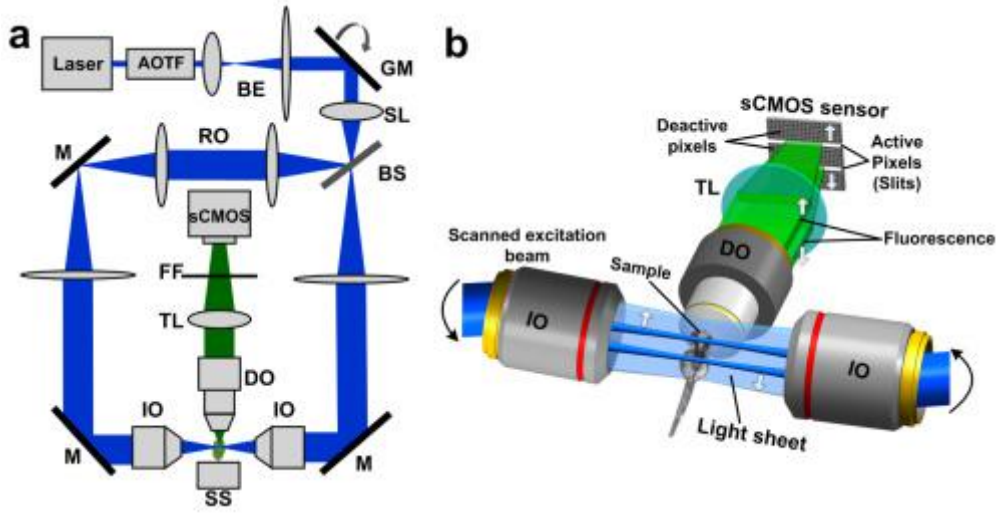


Figure 2.6 Schematic diagram of light sheet fluorescence microscopy and light pathways. (Yang et al., 2015)[50]

2.7 Optical m

2.7.1 Optical mapping of cardiac slices

Optical mappings were carried out for functional analysis. The responsiveness of the PdCMs in optogenetic mouse heart was measured. Slices were electrophysiologically assessed with the optical mapping method, using a custom-designed optical mapping system equipped with an EMCCD camera (Evolve 128 Photometrics, Tucson, USA). Slices were kept in Krebs solution containing 10μM blebbistatin at 37°C during imaging. Four 530nm LEDs were used for excitation of the Ca2+ -sensitive dye Rhod-2.

CaT fluorescence was collected at 585+/-40 nm. For Vm signals, four 530 nm LEDs were used for excitation of RH237, and emission was collected using a 662nm long pass filter. Vm and CaT measurements were taken at maximal resolution (128 x 128 pixels; pixel area 24 x 24 μm) at a rate of 1000 frames/sec. Slices were electrically stimulated with bipolar pulses of 2ms 9 duration, at voltages 1.5 times above threshold (5-10V) and initial frequency of 2Hz. For AP and CaT alternans investigations, slices were stimulated at 2, 4, 8 and 16 Hz frequency.

2.7.2 Data analysis and statistics

In the analysis of the continuous experimental data, values are reported as mean ± SEM of n experiments, and the observations were thought to be close to a normal distribution sufficiently to permit use of parametric tests. Paired or unpaired t tests were used as appropriate. All p values are 2 sided, the statistical software used to generate the results is SigmaStat software.

Chapter 3. Identification of a subtype of PdCMs possessing vesicular structures

3.1 Introduction

VMAT2 (ventricular monoamine transporter-2) is a known pharmacological target(Bernstein AI *et al.*, 2013) widely used to mark vesicles in the tissue. It has previously been used as a means to study cardiac neural structure (Dainius H.Pauza *et al.*, 2014). When investigating the possible function of PdCMs, I have discovered a novel structure in the ventricular tissue which is a bunch of gathered vesicles in some PdCMs in particular regions of the heart. To further clarify the structure and its location, I performed VMAT2/aACT co-staining using the z-stack function of the confocal microscope. I have found that the vesicular structure is located inside cardiomyocytes, usually close to the nucleus. Previous studies have indicated the existence of extra-cellular vesicular structure in the heart[29]. However, intra-cellular vesicular structure has not been reported yet. This finding suggests the functional importance of these vesicles in cardiac signaling, and provides instructive clues for cardiac research.

3.2 Results

3.2.1 VMAT2 staining on ventricular tissue

Shown on **figure 3.1** is the VMAT2 staining results. Different concentrations of VMAT2 antibody were applied on different tissue sections as is indicated by the figure legend. For immunostaining, GFP (1:1000) and Alexa 488(1:1000) were used as secondary antibodies respectively and confocal microscope was used to image the slides. For DAB-HRP staining, biotinylated secondary antibody (1:750) was applied to react with VMAT2 primary antibody and streptavidin-HRP/DAB chromogenic solution was used for precipitation. Adrenal gland was used as positive control to validate the VMAT2 antibody, negative control (without primary antibody) was also performed.

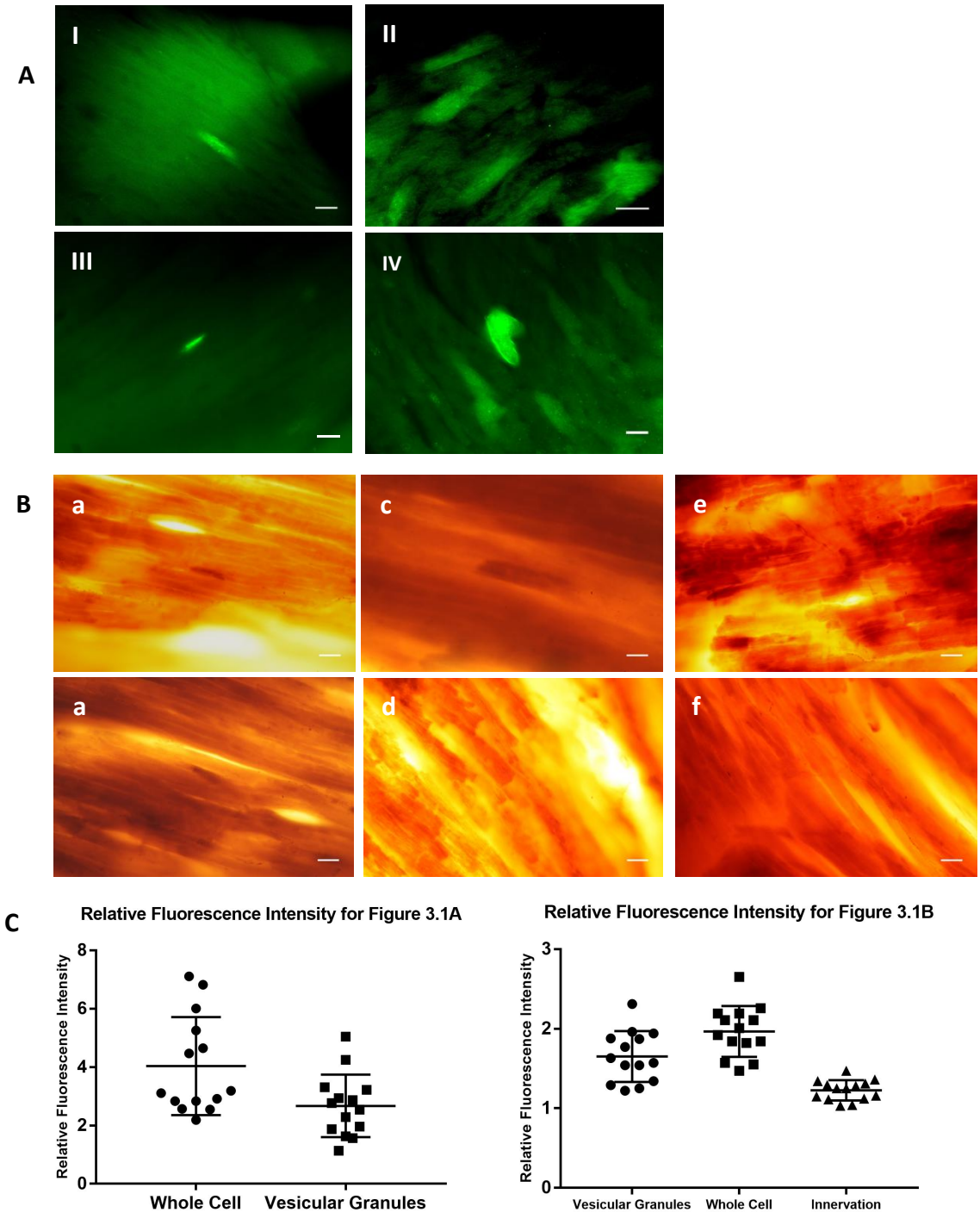


Figure 3.1 VMAT2 staining on ventricular tissue sections.

A. VMAT2(1:250) was applied to stained sliced heart tissue sections, Alexa488(1:1000) was used as secondary antibody. Images were taken from confocal microscope. Scale bar: 150μm. **I** and **II** show the vesicular granules, **III** and **IV** show the whole cell staining pattern. (n=13 preparations)

B. VMAT2(1:250) was stained with the ventricular tissue and HRP conjugated secondary antibody (1:750) was applied to react with VMAT2. DAB chromogenic solution was then applied to acquire brown precipitate. Images were obtained via optical microscope. Scale bar: 100 μ m. **a** and **b** show the vesicular granules, **c** and **d** show the whole cell staining pattern, **e** and **f** show the innervation pattern. n=17 preparations.

C. Relative fluorescence intensity for VMAT2 staining on ventricular tissue. The relative intensity was acquired by measuring the fluorescence intensity of positive stained area and then divided by the intensity of whole image. (n=14 selected regions)

The adrenal cortex structure was comparatively distinct, the Innervation in both left ventricle and right ventricle tissue was revealed by the fluoresce, as well, indicating the suitability of VMAT2 antibody to identify the innervation pattern in the heart.

The staining patterns could be divided into three categories, which are gathered vesicular granules, whole cell staining and neuronal innervation. In **Figure 3.1**A and 3.1B, I, III, a and b are representatives of the gathered vesicular granules, II, IV, c and d are defined as whole cell staining, while e and f are innervation patters.

Based on the three categories, I conducted the following experiments to further explore the VMAT2 staining patterns in the heart.

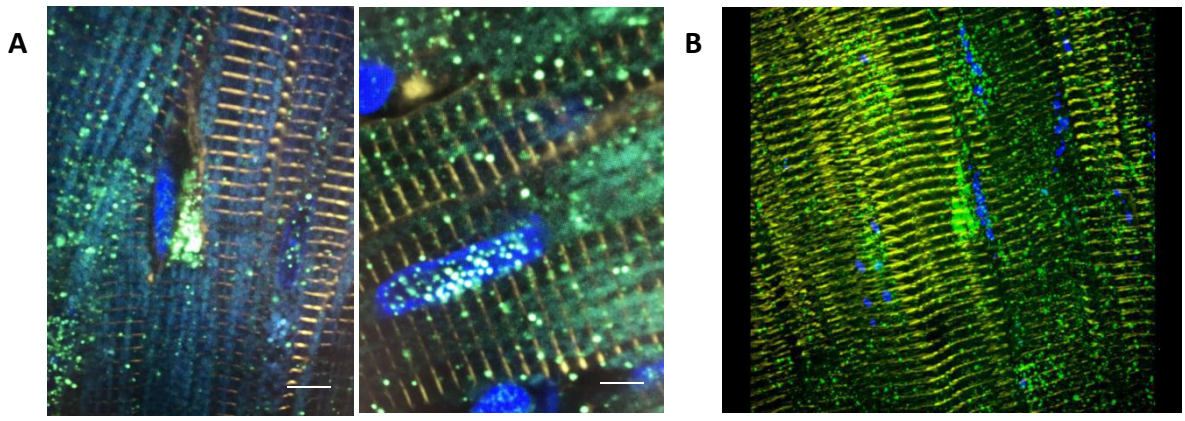
3.2.2 VMAT2/aACT co-staining on ventricular tissue

In order to identify the structure of VMAT2 stained regions and its relationship with cardiomyocytes, I used aACT(alpha-actinin) as a marker for cytoskeleton of myocytes. Therefore, VMAT2/aACT co-staining was perform on ventricular tissue sections and the slides were observed by confocal microscope.

Figure 3.2A are single layer merged co-staining images while **Figure 3.2**B is reconstructed 3D model. Both of them represents gathered vesicular granules.

The images taken from different fluorescent channels were in the same depth, indicating the cardiomyote boundaries of the particular regions.

Compared with innervation and whole cell staining, gathered vesicular granules worth key attention for its potential to discover a novel structure in cardiomyocytes. To confirm whether the vesicular structure is located within the myocytes, a series of z-stack images were taken under confocal microscope. The z-stack images were merged to be video 3, video 4 and video 5 shown in supplementary data.



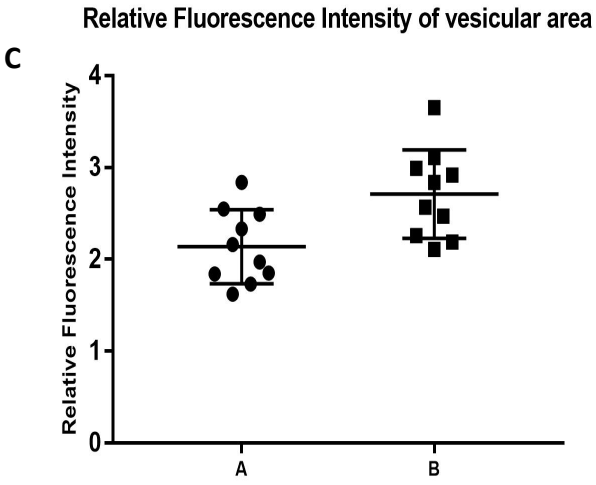


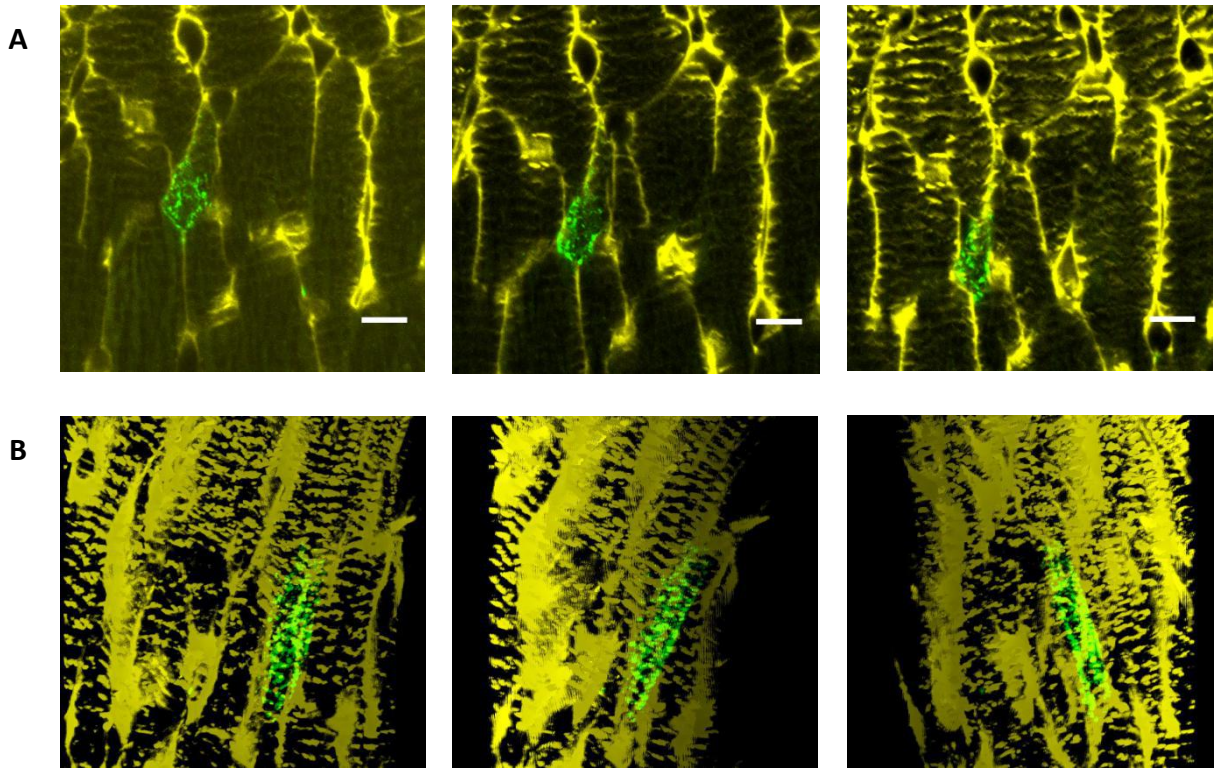
Figure 3.2 Reconstructed 3D model for VMAT2/aACT co-staining on ventricular tissue.

A. VMAT2(1:500) and aACT (alpha actinin 1:500) was applied on ventricle tissue sections, Cy3(1:1000) and Alexa488(1:1000) was used as secondary antibodies respectively. Nucleus was stained by DAPI. The images were obtained from different region of the slides via confocal microscope. Scale bar: 50μm.

B. Reconstructed 3D models for ventricular tissue. VMAT2(1:500) and aACT (alpha actinin 1:500) was applied on ventricle tissue sections, Cy3(1:1000) and Alexa488(1:1000) was used as secondary antibodies respectively. Nucleus was stained by DAPI. The images were obtained via confocal microscope.

C. Relative fluorescence intensity for VMAT2 staining on ventricular tissue. The relative intensity was acquired by measuring the fluorescence intensity of positive stained area and then divided by the intensity of whole image. (n=10 selected regions)

Most gathered vesicles in **Figure 3.2** were found to be localized near or around the nucleus. The vesicular structure, however, could not be concluded as intracellular location due to the imaging quality of the results. While in **Figure 3.3**, the vesicles were clearly identified to be located inside the myocyte, indicating the specific structure of monoamine vesicles inside the cardiomyocytes.



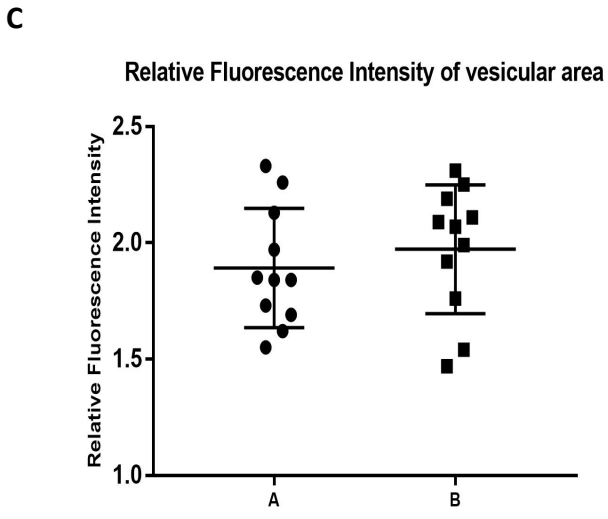


Figure 3.3 Intra-cellular vesicle structure by VMAT2/aACT co-staining

A. Series of z-stack images of VMAT2/aACT co-staining on ventricular tissue. VMAT2(1:250) and aACT (1:400) was applied on ventricle tissue sections, Cy3(1:1000) and Alexa488(1:1000) was used as secondary antibodies respectively. The images were obtained from the same region but different depth via confocal microscope. Scale bar: 50μm.

B. Reconstructed 3D models for z-stack images from figure 9A.

C. Relative fluorescence intensity for VMAT2 staining on ventricular tissue. The relative intensity was acquired by measuring the fluorescence intensity of positive stained area and then divided by the intensity of whole image. (n=11 selected regions)

3.3 Discussion

Extra-cellular vesicles in the heart are reported to play different roles in the heart in both physiological and pathological condition.

In my studies, I have proved the existence of the intra-cellular vesicular structure. Containing information molecules, intra-cellular vesicles are very likely to play similar roles with extra-cellular vesicles. VMAT2 stained vesicles, for instance, contain monoamines like dopamine and nor-adrenaline, which can be the mediator between sympathetic neurons and cardiomyocytes. There might also be possibilities that the vesicles may related to PdCMs, as has been previously hypothesized. These intra-cellular vesicles in the heart may have critical functions in sympathetic neuronal signaling, cardiomyocytes mediating and phenotype modification.

In future study, electron-microscopy is require to acquire higher resolution of the vesicular structure. Moreover, other markers for vesicles or monoamines are required for further staining. It would also be helpful to conduct some molecular experiments to quantify the expression level of related proteins.

Chapter 4. Identification of the innervation of sympathetic neuron and the distribution of EMT/VMAT transporters in the heart

4.1 Introduction

As has been introduced in Chapter 1, vesicular monoamine transporter (VMAT) is a transport protein which transports monoamine neurotransmitters into the vesicles, which release the neurotransmitters into synapses as chemical messages to post-synaptic neurons. VMAT2 has been widely used as the marker for vesicles and the pharmacological target[23,24]. Organic cation transporter 3 (OCT3) or Extra-neuronal monoamine transporter (EMT) is a protein that in humans is encoded by the SLC22A3 gene[13,14,15]. OCT3 is also reported to be expressing in the heart[16]. In the present studies, I also performed immunostaining using TH and OCT3 antibodies apart from VMAT2 to identify the innervation pattern in heart tissue as well as the distribution of monoamine transporters. The tissue was successfully stained and the innervation was clearly revealed. Furthermore, the existence of Extra-neuronal Monoamine Transporter (OCT3) in the heart was proved based on the staining pattern.

4.2 Results

4.2.1 TH immunostaining on ventricular tissue

Fresh heart was isolated from the mouse, followed by Langendorff perfusion and PFA fixation. Ventricular tissue slices were obtained by sectioning. TH (Tyrosine Hydroxylase) antibody was then applied on the ventricular tissue slices, combined with GFP secondary antibody. Adrenal gland and brain tissue sections were used as positive control for validating the antibody. During the staining

experiment, I attempted different concentrations for both primary antibody and secondary antibody, and finally optimized the concentrations to TH 1:500 and GFP 1:1000.

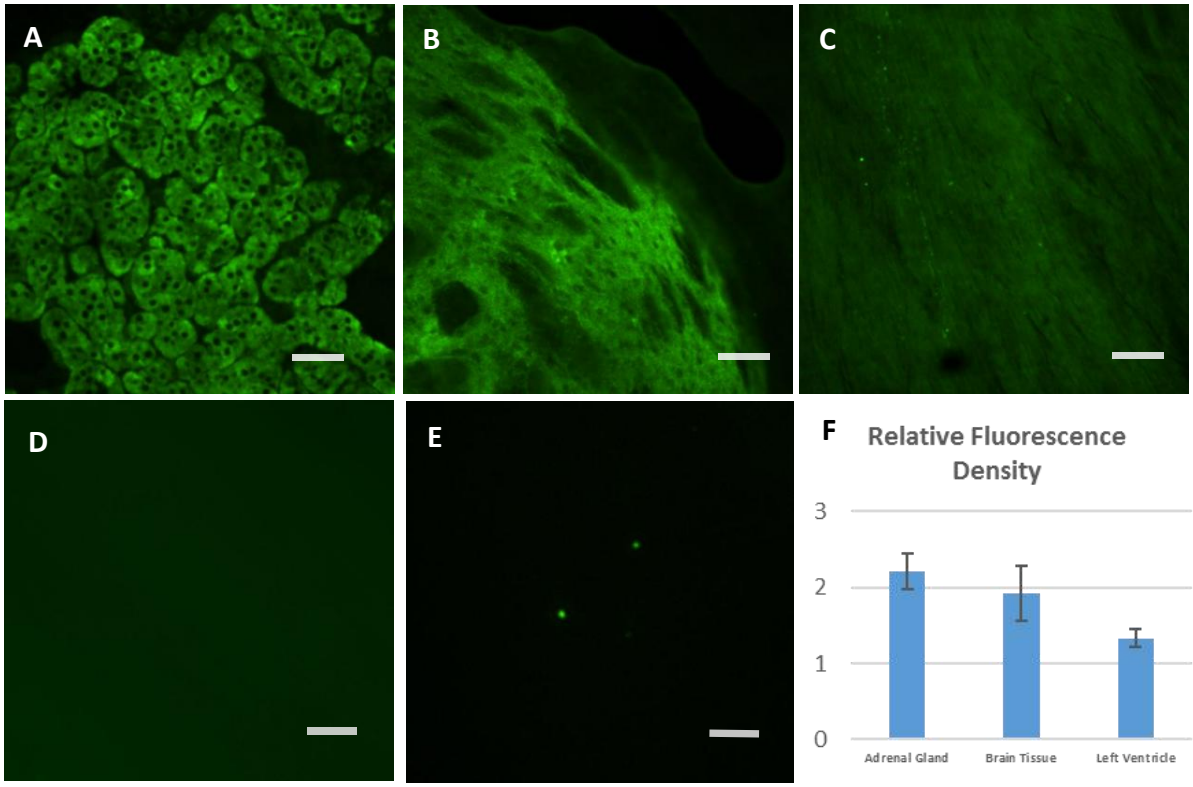


Figure 4.1 TH immunostaining on adrenal gland, brain and ventricular tissue. TH (Tyrosine Hydroxylase) was applied（1:500）on different tissue sections, GFP（1:1000）was used as secondary antibody and the images were obtained by spinning disk confocal microscope at 40X magnification. Scale bar: 200 μm.

A. Adrenal gland. (n=2 preparations)

B. Brain. (n=5 preparations)

C. Left ventricle. The positively stained neuronal fibre is marked by white arrows. (n=12 preparations)

D. Negative control for left ventricle tissue

E. Negative control for brain tissue

F. Relative fluorescence density of TH stained tissue sections. The relative fluorescence intensity was acquired by measuring the fluorescence density in positive stained region then divided by total fluorescence density. (n=15 selected regions)

The staining results indicates that Tyrosine Hydroxylase is a suitable marker for sympathetic nerve fibers in the heart and can be used to identify the innervation in murine heart. Shown on **Figure 4.1** are the immunostaining results of adrenal gland, brain tissue and ventricular tissue. According to the staining pattern of adrenal gland and brain, the antibody works properly. The adrenal cortex structure and neuronal structure are clearly displayed by the stained fluorescence. In ventricular tissue, the innervation of sympathetic nerves is revealed by the staining pattern. The nerve fibers are vertical spread as a whole,

according with the alignment of cardiomyocytes.

In **Figure 4.2**, two different kinds of innervation pattern were indicated by two kinds of antibody combination, which excluded the influence of fluorescent-crosstalk of the selected two secondary antibodies: Cy3 and GFP. The structure displayed by **Figure 4.2A** was not typical innervation pattern which might need further study.

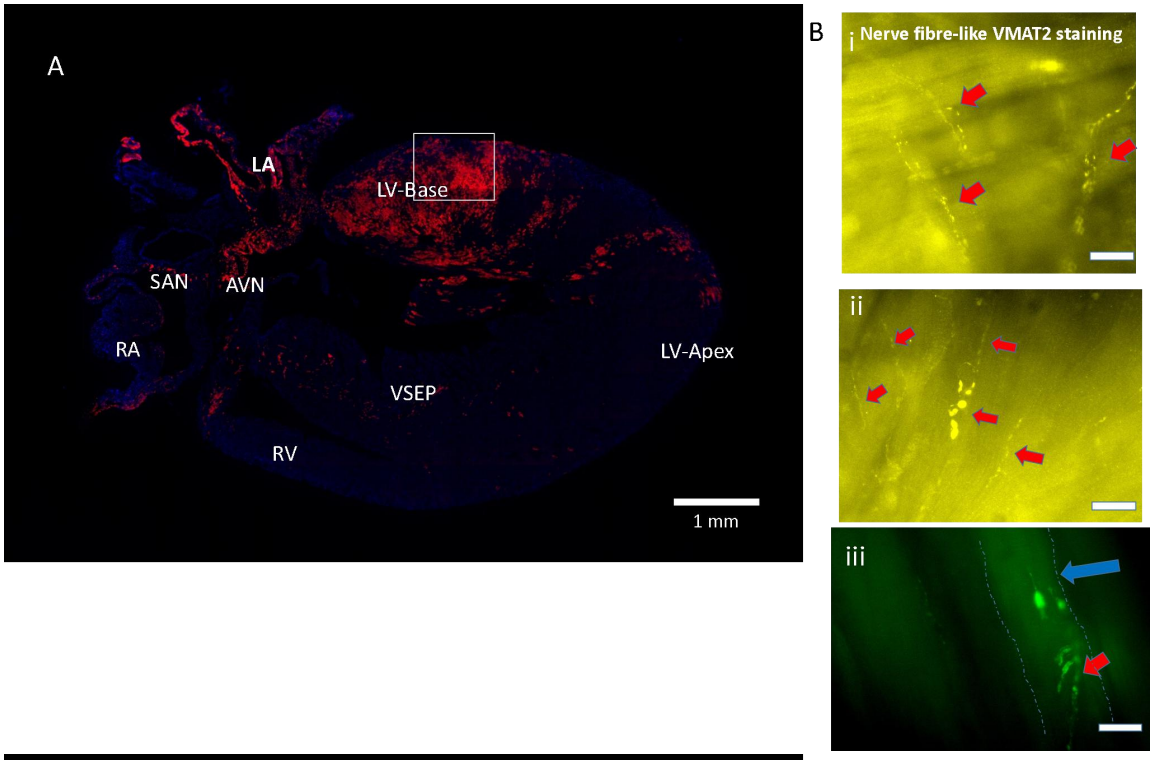


Figure 4.2 Innervation in heart tissue revealed by VMAT2 staining. **A:** A whole heart section histology imaging showing distribution PdCMs in different regions of a $Pnmt^{Cre/ChR2}$ heart**. B.** VMAT2(1:500) was applied on right ventricle tissue sections, GFP (1:1000) or Cy3(1:1000) was used as secondary antibodies respectively. The images were obtained via confocal microscope. Scale bar: 100μm. (n=7 preparations)

4.2.2 OCT3 immunostaining on ventricular tissue sections

The ventricular tissue sections were obtained by sectioning of fixed mouse heart. OCT3(extra-neuronal monoamine transporter) antibody was applied on the tissue sections, followed by GFP secondary antibody (1:1000) staining. The stained slides were then observed under wide-field microscope. Olfactory bulb tissue sections were used as positive control for validating the antibody. The overall staining quality on ventricular tissue was not as good as what I expected due to the low expression level. Therefore, a series of gradient concentrations were tested to achieve better staining quality. Consequently, the concentration of OCT3 antibody was fixed to 1:100.

As can be seen from **Figure 4.3**, the staining on olfactory bulb was comparatively acceptable. The cells located in both external plexiform layer and internal plexiform layer were stained by green fluorescence. The small granules located on the internal plexiform layer are preliminarily regarded as granule cell layer tissue.

However, whether the staining was membrane-located needs to be clarified by membrane marker fluorescence in future study to further validate the OCT3 antibody. Also, whether the small dots are granule cell layer tissue or dirty background requires further exploration by electron microscopy in future study.

As for the staining pattern of ventricular tissue, I could find multiple dots scattered around some specific area of the tissue. The staining quality was still not satisfying. In order to have a better view of the distribution pattern of extra-neuronal monoamine transporter, a video was produced based on a series of z-stack images.

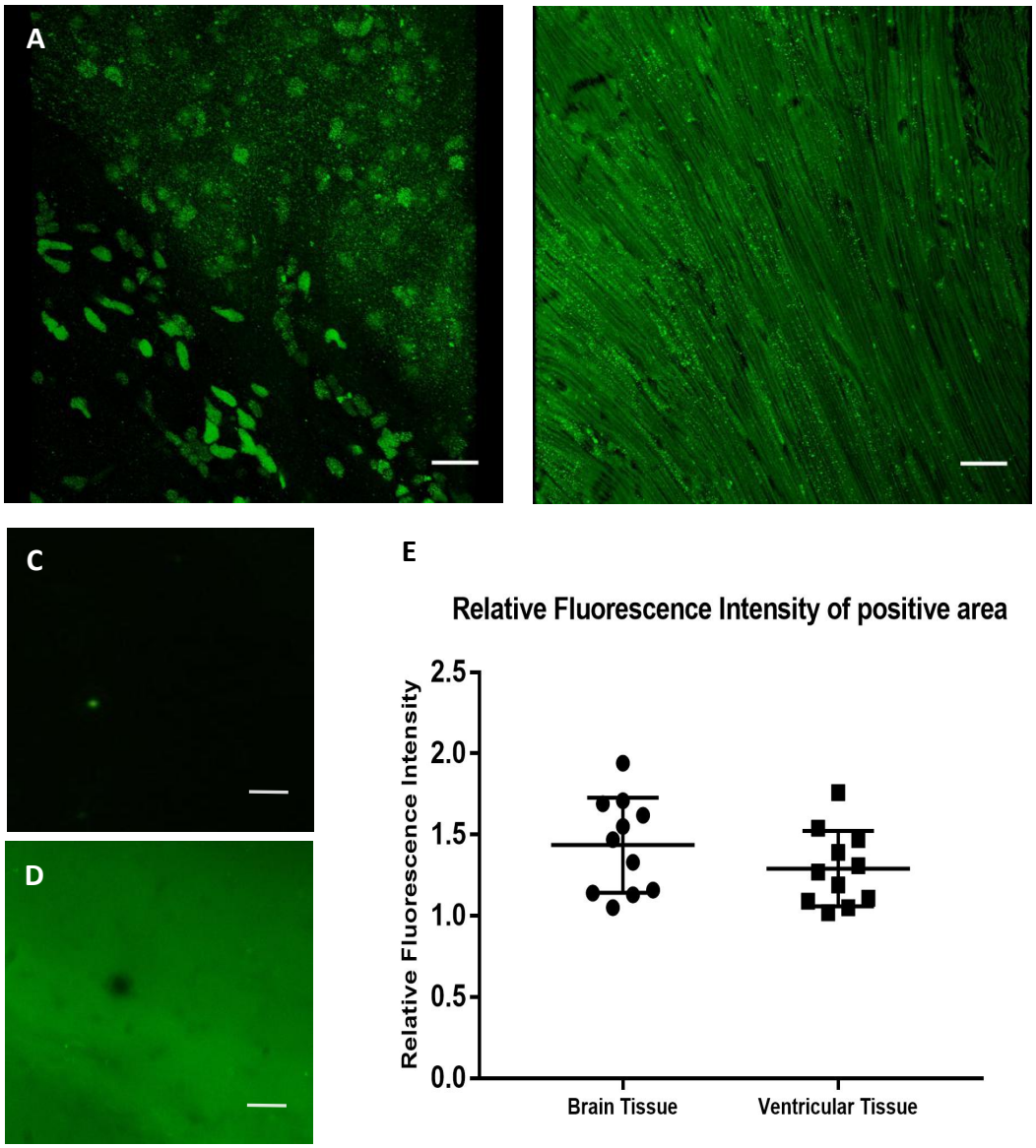


Figure 4.3 OCT3 immunostaining on Olfactry bulb and ventricular tissue sections (3D reconstructed model). OCT3(Extra-neuronal Monoamine Transporter SLC22A3) was applied (1:100) for staining and GFP (1:1000) was used as secondary antibody. The images were obtained by wide-field microscope. Scale bar: 20 μm.

A. Brain tissue section. (n=3 preparations)

B. Right ventricle section. (n=20 preparations)

C. Negative control for brain tissue.

D. Negative control for ventricular tissue.

E. Fluorescence ratio for OCT3 staining. The ratio was acquired by measuring the fluorescence density of selected positive area and the total density. The ratio was calculated by dividing the fluorescence density of selected area by the total density of the whole image. (n=11 selected regions)

4.3 Discussion

The expression of OCT3 in the heart tissue indicates the existence of extra-neuronal monoamine transporter and the uptake-2 mechanism in the heart.

Meanwhile, isolated cardiomyocytes were acquired by single cell isolation protocol. The cells were fixed and stained with OCT3/GFP antibodies with the same condition and then mounted as slides. The slides were observed under confocal microscope. However, no signal was found on these single cells. The supposed reasons were the low expression level as well as the structure broken during isolating the cells.

However, the clarity of the immunostaining method turned out to be insufficient and electron microscopy will be necessary in future study. Moreover, the assured structure was found for only once among a lot of preparations, the certainty of which requires further validation.

Similarly, isolated cardiomyocytes were fixed and stained with VMAT2/GFP antibodies with the same condition and then mounted as slides. The slides were observed under confocal microscope. However, no signal was found on these single cells, either. The supposed reasons could be the low expression level.

Chapter 5. Light-sheet Imaging study of the distribution and function study of PdCMs in Pnmt/ChR2 murine heart tissue by optogenetic stimulation

5.1 Introduction

In order to identify the distribution pattern of PdCMs, I conducted light-sheet microscopy imaging on cardiac tissue sections and reconstructed 3D models and galleries for better view. In addition, fucntional studies on Pnmt/ChR2 mouse hearts were performed using optical mapping. A series of values were measured including Calcium transient, trans-membrane potential, AP duration, activation time and amplitude, followed by statistic analysis.

5.2 Results

5.2.1 Light-sheet Imaging of atrial tissue dissected from $Pnmt^{Cre/ChR2}$ *heart*

The whole heart was isolated from optogenetic mice and thoroughly perfused with Langendorff perfusion system, followed by 4% PFA fixation. The atrial tissue was acquired by dissection under anatomical microscope and the tissue sections were stained with DAPI before taking images. Light-sheet microscope was used to obtain the images in different angles and different layers. The imaging was taken by Dr. Kate Wang.

As can be seen from **Figure 5.1A**, the PdCMs are distributed within the piece of tissue, and the red fluorescence is almost evenly scattered in the whole cells expressing tdTomato. We can therefore preliminarily conclude that ChR2/tdTomato is uniformly expressed in cytoplasmic matrix, and PdCMs are

widely distributed in atrial tissue of the heart. A three-dimensional model was built based on these light-sheet images to represent ChR2/tdTomato fluorescence. **Figure 5.1B** is a series of images merged as a gallery. Images taken from global angles clearly show the distribution pattern in this specific part of atrial tissue, indicating the suitability of tdTomato as a convenient fluorescence marker for cells expressing ChR2.

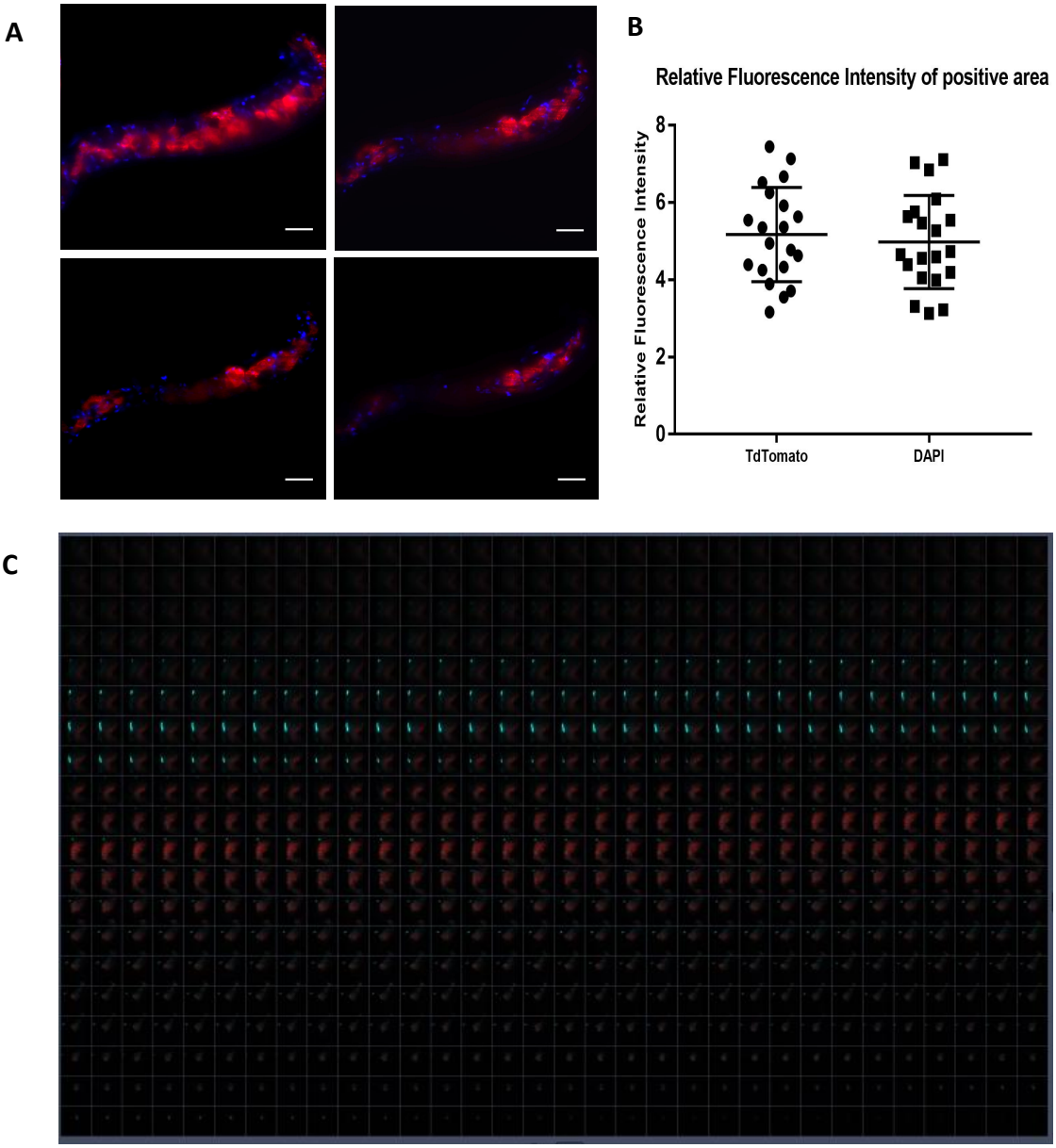


Figure 5.1 Light-sheet Imaging of atrial tissue dissected from Pnmt$^{Cre/ChR2}$ heart .

A. Images were taken from different angles using the light sheet microscope. Nucleus were stained with DAPI and and genetic expressing tdTomato was shown in red fluorescence. Scale bar: 50 μm. (n=2 preparations)

B. Relative Fluorescence Intensity for light-sheet images of optogenentic mouse atrial sections. The relative intensity was acquired by measuring the fluorescence density in selected area and then divided by total density. n=20

C. A series of light sheet images were merged as a gallery. (n=2 preparations). The images were taken by Dr. Kate Wang.

5.2.2 Optimisation of murine cardiac slice methodology

Adult murine ventricular slices have been previously developed for electrophysiology applications (Halbach et al., 2006), however optimization of the slice preparation to enable systematic analysis of Vm and CaT across the whole murine ventricles has yet to be achieved. **Figure 5.2** illustrates the methodology implemented in this study.

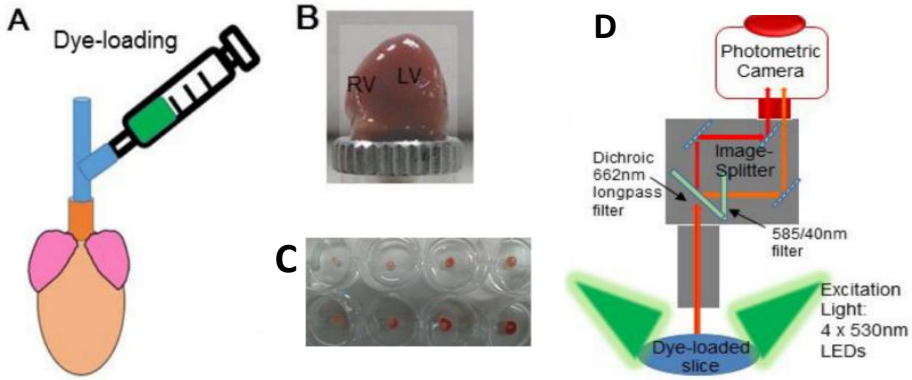


Figure 5.2 Optimization of murine cardiac slice methodology.

A: Voltage (RH237) or calcium (Rhod-2 AM) dyes were loaded via coronary circulation using the Langendorff perfusion system.

B: Ventricles were embedded in 4% low-melt agarose and mounted onto the vibratome specimen holder.

C: Slices were recovered at room temperature in Krebs solution containing 10 µM blebbistatin for 30 min, before optical mapping studies.

D: Optical mapping setup with four 530 nm excitation LEDs and a 128x128 EMCCD camera.

To achieve optimal dye loading, the voltage dye RH237 or Ca^{2+} dye Rhod-2 AM were loaded through the coronary circulation using the Langendorff perfusion system. Prevention of blood clot formation is essential for optimal dye loading and was achieved by initial injection of heparin (200 units) before animal sacrifice, and subsequent injection of streptokinase (400 units) directly into the coronary system after heart excision. Slices were cut at right angles to the long axis of the heart from the apex to the base, and 300 µm was found to be the best thickness to achieve optimal recordings for both Vm and CaT. After preparation, slices were pre-incubated at room temperature in Krebs solution containing 10 µM blebbistatin for an optimal recovery time of 30 min, prior to electrophysiological assessment using a custom-designed optical mapping system.

5.2.3 Vm and CaT measurements in Pnmt$^{Cre/ChR2}$ *ventricle slices*

After the optimization of the methodology, tans-membrane potential and Calcium transient measurements were conducted on prepared ventricle slices from optogenetic murine hearts by optical mapping.

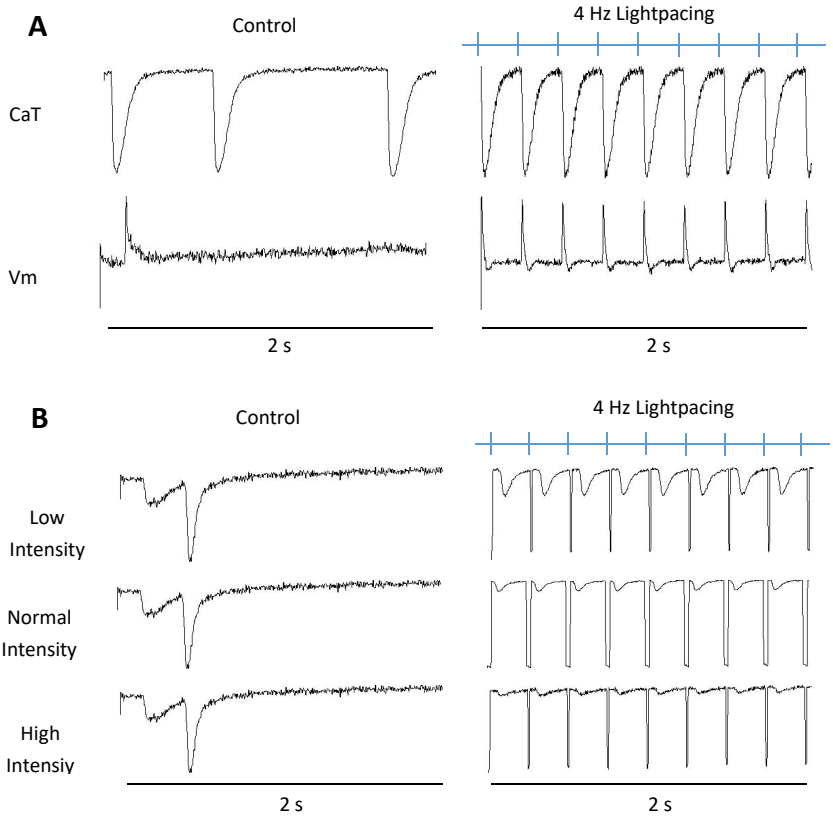


Figure 5.3 Vm and CaT measurements in murine ventricle slices. **A**: CaT and Vm obtained from ventricle slices under 4Hz pacing frequency. Scale bar: 2s. (n= 3 hearts) **B**: CaT signals obtained from the murine ventricle slices with different light intensities at 4Hz pacing frequency. Scale bar: 2s. (n= 4 hearts)

As is shown in **Figure 5.3**A, CaT and Vm were obtained from ventricle slices under 4Hz lightpacing. In comparison to the control, in which the heart rhythm was irregular, the heart tissue was successfully paced by blue light stimulation accorded to the pacing frequency.

In **Figure 5.3**B, Calcium transient was recorded under three different light intensities. The heart tissue slices were able to be paced under 4Hz light stimulation. According to the gradient of light intensity, higher intensity indicated higher Calcium transient value while lower intensity for lower value. The pattern of the waveforms was different when analyzing different regions.

Shown on **Figure 5.4** is the APD75ms analysis of the three different light intensity gradients, respectively. We can find that higher intensity indicates higher activity of AP amplitude, which accords with my hypothesis.

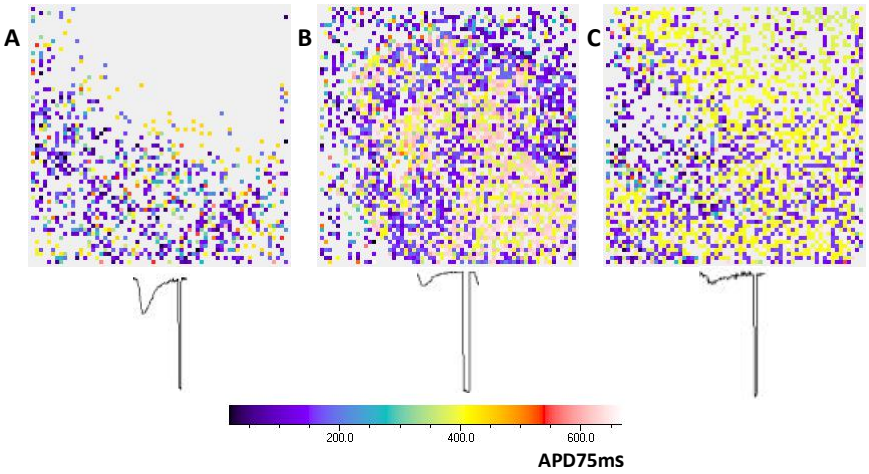


Figure 5.4 Transmural and regional distribution of AP duration under different light intensity stimulation. APF75ms analysis was performed based on the three different light intensity gradients of 4Hz. **A.** Low intensity. **B.** Medium intensity. **C.** High intensity. (n=4 hearts)

As shown in **Figure 5.5**, Optogenetic pacing of PdCMs can establish an alternative pacing site in murine atria. Thus, selectively stimulating PdCMs with rhythmic blue light (470nm) pulses was sufficient to overdrive the sinus rhythm, supporting previous observations from whole heart studies. It has also been found previously that the left atrium – dissected out by itself – can be paced by light, but it has not been tested in sinoatrial preparations. In 3 out of the 10 sinoatrial preparations tested, I found a marked change in the tissue activation pattern. In the example depicted here, prior to pacing the first region to activate is in the region of the SAN (**Figure 5.5** left), whereas once pacing is applied a second, artificial pacing site is set up on the septal border of the left atrial side of the preparation.

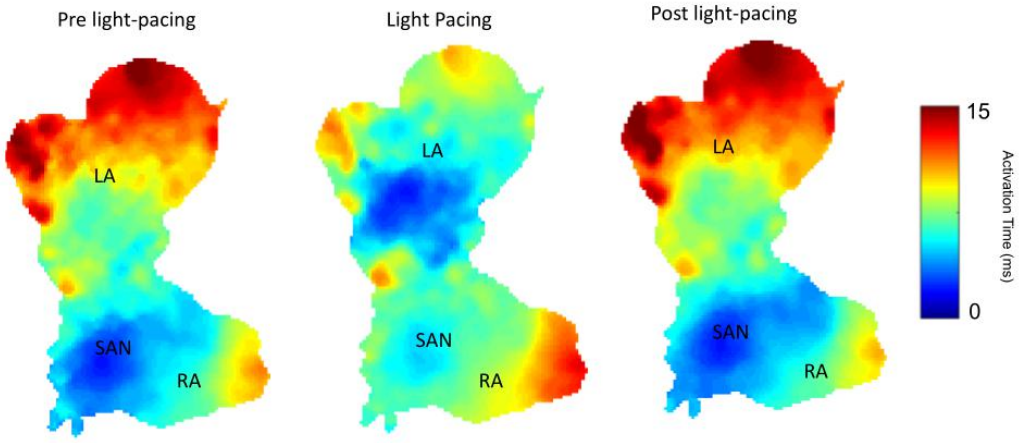


Figure 5.5 Activation patterns for before and during optogenetic pacing. Left: Activation map from before optogenetic pacing (scale bar on right). Middle: Activation map of the same specimen, during optogenetic pacing. Right: Activation map after optogenetic pacing Note that the site of earliest activation has shifted from the SAN area in the bottom (n=10 sinoatrial preparations examined).

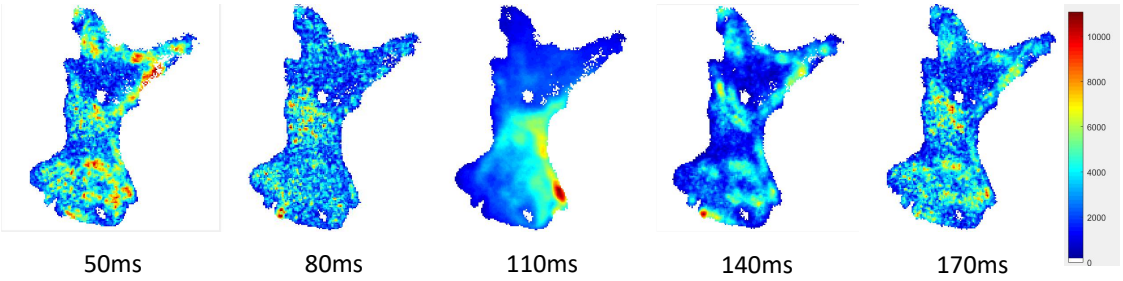


Figure 5.6 Amplitude Maps for Sinus node 200ms pacing. Amplitude of isolated sunus node sections was measured and analyzed by Electro-maps(Version 2.1). The amplitude patterns of different time points after pacing were shown on the figure. Scale bar is on the right side. (n=5 preparations)

5.3 Discussion

Based on the optic mapping results shown above, Pnmt/ChR2 expressing murine heart ccould be successfully paced using light stimulation, indicating the optimized mapping system could be a useful tool for optogenetic studies. The pacing results verified the genotype of our mouse model. As for the activation patterns, we can clearly observe that the activation time was decreased on the whole tissue and the most activated region switched from sinus node to left atrial, which indicates the electro-physiological cardiac signaling state in heart beating. The amplitude maps show the status of sinus node during light pacing. Both activation maps and amplitude maps are produced using the software Electro-Maps(from Birmingham University), and the maps could give an intuitionistic display on tissue status, which could be very helpful in future studies.

Chapter 6. Discussion

6.1 Optimization of the genotyping protocol

The protocol for genotyping has been used for years in our lab. However, when I performed genotyping for many times, I have found that the quantity and quality of PCR products could alter due to the change of some conditions. Therefore, I optimized the genotyping protocol by changing the concentration of the DNA extraction product and the dissolving temperature.

As for making agarose gel for electrophoresis, removing air bubbles proves to be rather important to acquire a better imaging quality. After pouring the gel mixture into the mould, the larger side of a 1ml tip will be very useful to remove the bubbles.

For running the gel on electrophoresis, the 100V constant voltage could be optimized by 20mA constant current, which performs a more stable and orderly band.

6.2 Distribution of PdCMs by light-sheet imaging

As can be seen in the results part, the tdTomato fluorescence is evenly scattered in the whole cell, which accords with previous study in our lab (Wang Y *et al., 2017*). The staining pattern the myocytes indicates that in our mouse model, ChR2(Nagel *et al., 2003*) is intra-cellular expressed in the myocytes. As for the overall distribution pattern of PdCMs in the atrial tissue, it can be seen that the percentage of Pnmt expressing cells is approximately 50%, indicating its important role in such specific regions. According to our previous study, the PdCMs are predominantly expressed in the left side of the heart, which accords with other reported findings (Osuala *et al.*, 2011). However, the reason why PdCMs are located in these particular regions remains unknown.

It was previously shown that adrenergic deficiency led to impaired electrical conduction and increased arrhythmic potential in embryonic mouse heart(Baker C *et al.*, 2012). The established mouse line provide a valuable functional tool for the study of the physiological properties of PdCMs.

The limitation of our study is that only a small region of atrial tissue was examined, which cannot give a whole heart imaging result. The reasons for not doing a whole heart staining was that the transparency of the heart could not satisfy the requirement for light-sheet imaging and the refractive index did not match well. Furthermore, the tissue has not been cleared for a better staining condition. In future study, successfully performed tissue clearing should be involved for whole heart staining and other antibodies such as HCN4, VMAT2, OCT3, and TH should be included to explore the relation between PdCMs and sympathetic nerve system.

6.3 OCT3 and TH staining on ventricular tissue sections

The innervation pattern in the heart has been reported over the years (Hildreth V *et al.*, 2009 and Shoba T *et al.*, 2000). The TH staining in my experiments successfully indicated sympathetic neuron innervation in local cardiac regions. In adrenal gland and brain tissue, the antibody was well-stained.

OCT3, also known as extra-neuronal monoamine transporter (Kekuda R *et al.*, 2009), represent the uptake-2 mechanism for nor-adrenaline. I supposed a model that PdCMs works as a mediator between sympathetic neurons and conventional cardiomyocytes for absorbing released nor-adrenaline by uptake-2 and transverse nor-adrenaline to adrenaline. Based on my hypothesis, OCT3 should be expressed on membrane of most PdCMs. In the imaging result, however, I could not see clearly whether OCT3 was membrane-located because of the lack of membrane marker. Moreover, the overall expression level of OCT3 was low in the heart, and the stained spots did not show a distinct pattern. Also, there was no direct co-relation found between PdCMs and OCT3 expressing cells.

In this part, single cell staining of OCT3 was also performed, with no fluorescence signal found. The reasons, as I suggest, are that there would be cell damage occurred when conducting cell isolation, and the possibility to acquire

the positive cells is low due to the expression level.

Since the OCT3 staining failed to give a convincing evidence, further study is necessary. To optimize the experimental plans, flow-cytometry can be applied to select positive cells before staining and imaging.

6.4 VMAT2/aACT staining on cardiac tissue sections and cellular vesicles

In my study, VMAT2 staining pattern can be divided into three categories, whole cell staining, innervation and gathered vesicles. Innervation is the most common pattern in heart tissue, which is consistent with the TH staining pattern. Whole cell staining is also quite common, particularly in the regions close to ventricle and atrium. Similar staining pattern has been reported in adrenergic cardiomyocytes (Ravi C. Balijepalli *et al.*, 2006). Intra-cellular vesicular structure, however, has not been reported yet.

To further investigate the location of these vesicles, I applied a-ACT as the marker for myocytes, which method has been widely used (C. Blake Nichols *et al.*, 2010). In the z-stack images of VMAT2/aACT co-staining, it can be testified that the clustered vesicles are located inside myocytes, especially near the nucleus. In previous study, this vesicular structure only exists in neuron cells responsible for vesicular transport for monoamines. The present findings may provide clues for a new type of myocyte which plays an important role on sympathetic neuronal signal transduction.

In future study, electron microscope should be involved to acquire distinct resolution on particular vesicles. Also, other antibodies such as dopamine/nor-adrenaline related proteins should be applied to co-stain with VMAT2 for verification.

Extra-cellular vesicles in the heart are widely reported to mediate different ischemic preconditioning (Giricz Z *et al.*,2014), heart failure(Kervadec A *et al.*,2016) and infarcted heart(Chistiakov DA *et al.*,2016). People have proved that cardiac extra-cellular vesicles play a crucial role in both pathology and physiology(Gaceb A *et al.*,2014). These vesicles represent a new way to convey

information between cells such as proteins, second messengers and genetic information to modify the phenotype and function of the target cells. In comparison to extra-cellular vesicles, intra-cellular vesicles have not been reported to exist in the heart.

In the present findings, however, intra-cellular vesicles are very likely to present in cardiac tissue, even in cardiomyocytes. There is no doubt that such vesicles contain information molecules and play similar roles with extra-cellular vesicles to some degree. VMAT2 stained vesicles, for instance, contain monoamines like dopamine and nor-adrenaline, which can be the mediator between sympathetic neurons and cardiomyocytes, or conventional cardiomyocytes and adrenergic myocytes. Even further, the VMAT2 stained vesicles may related to PdCMs, as I previously hypothesized. Therefore, we can suggest that similar to extra-cellular vesicles, these intra-cellular vesicles in the heart may have critical functions in sympathetic neuronal signaling, cardiomyocytes mediating and phenotype modification. The functions of these intra-cellular vesicles located in cardiomyocytes worth intensive study and are very likely to provide a wide and bright prospective.

6.5 Optic mapping on heart tissue

Optic mapping has been used for structural and functional studies of animal hearts for a long time (Wang *et al*., 2015; Halbach *et al*., 2006). In this experiment, I performed CaT and Vm measurement with high resolution mapping, followed by AP duration analysis.

Under 4Hz stimulation, the heart tissue was successfully paced and accomplished 9 consistent beats in 2 seconds. This suggests that our mouse model is suitable for optogenetic study and functional analysis on PdCMs. Based on the results, both CaT and Vm are correctly measured and show consistency to my anticipation. It can be clearly seen that the waveforms under different light intensity also show accordance. As for APD analysis, higher light intensity brings more activated regions and longer average AP duration. The area of longer duration expands with the increase of intensity. The activation maps and amplitude maps indicated the electro-physiological signaling status of the heart

tissue, particularly sinus node.

6.6 Conclusion and future prospective

The key findings of this report include: i) firstly, a subtype of PdCMs possesses vesicular structure was revealed by using immunostaining of vesicular monoamine transporter 2 (VMAT2) and myocyte marker α-actinin (aACT) as well as extra-neuronal monoamine transporter (EMT/ OCT3). This is the first time that such cellular vesicles have been found in cardiomyocytes. Although such vesicular structure requires further investigation, it opens a new frontier for exploring the cardiomyocyte endocrine function; ii) secondly, a synapse-like junction structure between these cardiomyocytes and sympathetic neuron innervation was identified by the staining of anti-Tyrosine Hydroxylase(TH) and anti-VMAT2; iii) finally, by using optogenetic stimulation combining with a high resolution optical imaging, the potential role as alternative pacemaker site of PdCMs was explored, which was induced by optogenetic pacing technique.

Thus, the results presented in my report have provided novel evidence to suggest the endocrine function and the pivotal role in neurocardial crosstalk of PdCMs.

References

1. Goldstein, M; Fuxe, K; Hökfelt, T. Characterization and tissue localization of catecholamine synthesizing enzymes. Pharmacological Reviews. 24 (2): 293 –309. PMID 4564603 (1972).

2. Sineshchekov OA, Jung KH, Spudich JL. Two rhodopsins mediate phototaxis to low- and high-intensity light in Chlamydomonas reinhardtii. Proc. Natl. Acad. Sci. U.S.A. 99 (13): 8689 –94. doi:10.1073/pnas.122243399. PMC 124360. PMID 12060707 (2002).

3. Wang Y, Lin WK, et.al. Optogenetic Control of Heart Rhythm by Selective Stimulation of Cardiomyocytes Derived from Pnmt+ Cells in Murine Heart. Scientific Reports. doi: 10.1038/srep40687. PMC 5234027. PMID 28084430 (2017).

4. White I. A., Gordon J., Balkan W. & Hare J. M. Sympathetic reinnervation is required for mammalian cardiac regeneration. Circ Res 117, 990 –994 (2015).

5. Garikipati V. N. S., Verma S. K. & Kishore R. The nervous heart: role of sympathetic reinnervation in cardiac regeneration. Circ Res 117, 980 –981 (2015).

6. Tamura Y. et al. Neural crest-derived resident cardiac cells contribute to the restoration of adrenergic function of transplanted heart in rodent. Cardiovasc Res 109, 350 –357 (2016).

7. Lieberman M, Marks A, Peet A. Marks' Basic Medical Biochemistry: A Clinical Approach (4th ed.). Philadelphia: Wolters Kluwer Health/Lippincott Williams & Wilkins. p. 175. ISBN 9781608315727. (2013)

8. Bell DR. Medical physiology: principles for clinical medicine (3rd ed.). Philadelphia: Lippincott Williams & Wilkins. p. 312. ISBN 9780781768528. (2009)

9. Khurana. Essentials of Medical Physiology. Elsevier India. p. 460. ISBN 9788131215661. (2008)

10. Rang HP, Ritter JM, Flower R, Henderson G. "Chapter 14: Noradrenergic transmission". Rang & Dale's Pharmacology. Elsevier Health Sciences. pp. 177 –196. ISBN 978-0-7020-5497-6. (2014)

11. Derek Waller, Tony Sampson. "Chapter 4: Neurotransmission and the peripheral autonomic nervous system". Medical Pharmacology. 5th edition. ISBN: 9780702071676. (2017)

12. Kaumann AJ, Hall JA, Murray KJ, Wells FC, Brown MJ. A comparison of the effects of adrenaline and noradrenaline on human heart: the role of beta 1- and beta 2-adreanaline receptors in the stimulation of adenylate cyclase and contractile force. Eur Heart J. 10 Suppl B:29-37. (1989)

13. Kekuda R, Prasad PD, Wu X, Wang H, Fei YJ, Leibach FH, Ganapathy V. Cloning and functional characterization of a potential-sensitive, polyspecific organic cation transporter (OCT3) most

abundantly expressed in placenta. J Biol Chem. 273 (26):
15971 –9. doi:10.1074/jbc.273.26.15971. PMID 9632645. (1998).

14. Verhaagh S, Schweifer N, Barlow DP, Zwart R. Cloning of the mouse and human solute carrier 22a3 (Slc22a3/SLC22A3) identifies a conserved cluster of three organic cation transporters on mouse chromosome 17 and human 6q26-q27. Genomics. 55 (2):
209 –18. doi:10.1006/geno.1998.5639. PMID 9933568.(1999)

15. Hayer-Zillgen M, Brüss M, Bönisch H. Expression and pharmacological profile of the human organic cation transporters hOCT1, hOCT2 and hOCT3. Br J harmacol. 136 (6): 829 –836. doi: 10.1038/sj.bjp.0704785. PMC 1573414. PMID 12110607. (2002)

16. Solbach TF, Grube M, Fromm MF, Zolk O.Organic cation transporter 3: expression in failing and nonfailing human heart and functional characterization. J Cardiovasc Pharmacol. 58(4):409-17. doi: 10.1097/FJC.0b013e3182270783. (2011)

17. Fowler JS1, Logan J, Shumay E, Alia-Klein N, Wang GJ, Volkow ND.Monoamine oxidase: radiotracer chemistry and human studies. J Labelled Comp Radiopharm. 2015 Mar;58(3):51-64. doi: 10.1002/jlcr.3247. (2015)

18. Morris RG1, Venning MG, de la Lande IS.Influence of uptake1 and uptake2 on the relationship between diffusion and metabolism of noradrenaline in the perfused rabbit ear artery. Blood Vessels. 25(5):217-31. (1988)

19. Bryan LJ, O'Donnell SR.Kinetic analyses of the mechanisms of action of inhibitors of the extraneuronal uptake of adrenaline in smooth muscle cells of guinea-pig trachea. Naunyn Schmiedebergs Arch Pharmacol. 315(3):249-54. (1981)

20. Grohmann M, Trendelenburg U.The substrate specificity of uptake2 in the rat heart. Naunyn Schmiedebergs Arch Pharmacol. 328(2):164-73. (1984)

21. Eiden L.; Schäfer M. H.; et al. The vesicular amine transporter family (SLC18) amine/proton antiporters required for vesicular accumulation and regulated exocytotic secretion of monoamines and acetylcholine. Pflügers Archiv. 447 (5):
636 –640. doi:10.1007/s00424-003-1100-5. PMID 12827358. (2004)

22. Wimalasena K. Vesicular monoamine transporters: structure-function, pharmacology, and medicinal chemistry. Med Res Rev. 31 (4):
483 –519. doi:10.1002/med.20187. PMC 3019297 . PMID 20135628. (2011)

23. Bernstein AI, Stout KA, Miller GW. The vesicular monoamine transporter 2: an underexplored pharmacological target. Neurochem Int. 2014 Jul; 73:89-97. doi: 10.1016/j.neuint. (2014)

24. Nickell JR, Siripurapu KB, Vartak A, Crooks PA, Dwoskin LP. The vesicular monoamine transporter-2: an important pharmacological target for the discovery of novel therapeutics to treat

methamphetamine abuse. Adv Pharmacol. 69:71-106. doi: 10.1016/B978-0-12-420118-7.00002-0. (2014)

25. Pauza DH, Rysevaite-Kyguoliene K, Vismantaite J, Brack KE, Inokaitis H, Pauza AG, Rimasauskaite-Petraitienė V, Pauzaite JI, Pauziene N.A combined acetylcholinesterase and immunohistochemical method for precise anatomical analysis of intrinsic cardiac neural structures. Ann Anat. 196(6):430-40. doi: 10.1016/j.aanat.2014.08.004. (2014)

26. Mulcahy LA, Pink RC, Carter DR. Routes and mechanisms of extracellular vesicle uptake. J Extracell Vesicles. 2014 Aug 4;3. doi: 10.3402/jev. v3.24641. (2014)

27. Fertig ET, Gherghiceanu M, Popescu LM.Extracellular vesicles release by cardiac telocytes: electron microscopy and electron tomography.J Cell Mol Med. 18(10):1938-43. doi: 10.1111/jcmm.12436. (2014)

28. Giricz Z, Varga ZV, Baranyai T, Sipos P, Pálóczi K, Kittel Á, Buzás EI, Ferdinandy P5.Cardioprotection by remote ischemic preconditioning of the rat heart is mediated by extracellular vesicles. J Mol Cell Cardiol. 2014 Mar;68:75-8. doi: 10.1016/j.yjmcc.2014.01.004. (2014)

29. Gaceb A, Martinez MC, Andriantsitohaina R2.Extracellular vesicles: new players in cardiovascular diseases. Int J Biochem Cell Biol. 2014 May; 50:24-8. doi: 10.1016/j.biocel.2014.01.018. (2014)

30. Pfeifer P, Werner N, Jansen F.Role and Function of MicroRNAs in Extracellular Vesicles in Cardiovascular Biology. Biomed Res Int. 2015; 2015:161393. doi: 10.1155/2015/161393. (2015)

31. Chistiakov DA, Orekhov AN, Bobryshev YV. Cardiac Extracellular Vesicles in Normal and Infarcted Heart. Int J Mol Sci. 2016 Jan 5;17(1). pii: E63. doi: 10.3390/ijms17010063. (2016)

32. Bank IE, Timmers L, Gijsberts CM, Zhang YN, Mosterd A, Wang JW, Chan MY, De Hoog V, Lim SK8, Sze SK, Lam CS, De Kleijn DP. The diagnostic and prognostic potential of plasma extracellular vesicles for cardiovascular disease. Expert Rev Mol Diagn. 2015;15(12):1577-88. doi: 10.1586/14737159.2015.1109450. (2015)

33. Coote JH1, Chauhan RA2. The sympathetic innervation of the heart: Important new insights. Auton Neurosci. 2016 Aug;199:17-23. doi: 10.1016/j.autneu.2016.08.014. (2016)

34. Kreipke RE, Birren SJ. Innervating sympathetic neurons regulate heart size and the timing of cardiomyocyte cell cycle withdrawal. J Physiol. 2015 Dec 1;593(23):5057-73. doi: 10.1113/JP270917. (2015)

35. Scientists at UCLA and Caltech generated this image of the nerves in a mouse's heart. Credit: UCLA/Caltech

https://www.eurekalert.org/multimedia/pub/129927.php

36. Deisseroth, K.; Feng, G.; Majewska, A. K.; Miesenbock, G.; Ting, A.; Schnitzer, M.

J. Next-Generation Optical Technologies for Illuminating Genetically Targeted Brain Circuits. Journal of Neuroscience. 26 (41):
10380 –6. doi:10.1523/JNEUROSCI.3863-06.2006. PMC 2820367. PMID 17035522. (2006)

37. Boyden E. S., Zhang F., Bamberg E., Nagel G. & Deisseroth K. Millisecond-timescale, genetically targeted optical control of neural activity. Nat Neurosci 8, 1263 –1268 (2005).

38. Jia Z. et al. Stimulating Cardiac muscle by light: cardiac optogenetics by cell delivery. Circ: Arrhythm Electrophysiol 4, 753 –760 (2011).

39. Park S. A., Lee S.-R., Tung L. & Yue D. T. Optical mapping of optogenetically shaped cardiac action potentials. Sci. Rep 4, doi: 10.1038/srep06125 (2014).

40. *Bingen B. O. et al. Light-induced termination of spiral wave arrhythmias by optogenetic engineering of atrial cardiomyocytes. Cardiovasc Res 104, 194 –205 (2014).*

41. JR Blueford. "Lesson 2 — Page 3, CLASSIFICATION OF MICROSCOPES". msnucleus.org. Archivedfrom the original on 10 May 2016. Retrieved 15 January 2017.

42. Zeiss Education in Mircroscopy and Digital Imaging.
http://zeiss-campus.magnet.fsu.edu/articles/basics/opticaltrain.html

43. Pawley JB (editor) (2006). Handbook of Biological Confocal Microscopy (3rd ed.). Berlin: Springer. ISBN 0-387-25921-X.

44. *https://en.wikipedia.org/wiki/Confocal_microscopy#cite_note-Pawley_2006-1*

45. *http://zeiss.magnet.fsu.edu/tutorials/spinningdisk/yokogawa/yokogawatutorialfigure1.jpg*

46. http://zeiss.magnet.fsu.edu/tutorials/spinningdisk/yokogawa/yokogawatutorialfigure1.jpg

47. "Das erste deutsche Fernsehpatent von Paul Nipkow". PC Magazin. 30 June 2015. Retrieved 28 April 2017.

48. http://www.bristol.ac.uk/synaptic/research/techniques/widefield.html

49. T.C. Fadero et al. "LITE microscopy: Tilted light-sheet excitation of model organisms offers high resolution and low photobleaching" 2018. Journ. Cell Biol. *DOI: 10.1083/jcb.201710087 (2018)*

50. Z Yang, L Mei et al. Dual-slit confocal light sheet microscopy for in vivowhole-brain imaging of zebrafish. Biomedical Optics Express. Vol. 6, Issue 5, pp. 1797-1811. (2015)

51. C Ding, T H Everett. Assessment of Cardiac Conduction: Basic Principles of Optical Mapping. Methods in molecular biology (Clifton, N.J.) 660:239-52. (2010)